Effect of processing conditions on the properties of vitrimerized polybutylene terephthalate prepared by reactive extrusion

Quentin-Arthur Aimé Q.-A. Poutrel POUTREL, R. Kmo, A. Cohadon, Julien Boisse, S. Rouzière, Stéphane André, Sandrine Hoppe, Laurent Farge

Effect of processing conditions on the properties of vitrimerized polybutylene terephthalate prepared by reactive extrusion

Q.-A. Poutrel[1,2,*], R. Kmo[1], A. Cohadon[2], J. Boisse[1], S. Rouzière[3], S. André[1], S. Hoppe[2], L. Farge[1]

[1]Université de Lorraine, CNRS, LEMTA, F-54000 Nancy, France

[2]Université de Lorraine, CNRS, LRGP, F-54000 Nancy, France

[3]Laboratoire de Physique des Solides, CNRS, Université Paris-Sud, Université Paris-Saclay, 91400 Orsay, France

Corresponding author:

Mail: *quentin-arthur.poutrel@univ-lorraine.fr*

Postal address: *1 rue Grandville, LRGP, 54000, Nancy*

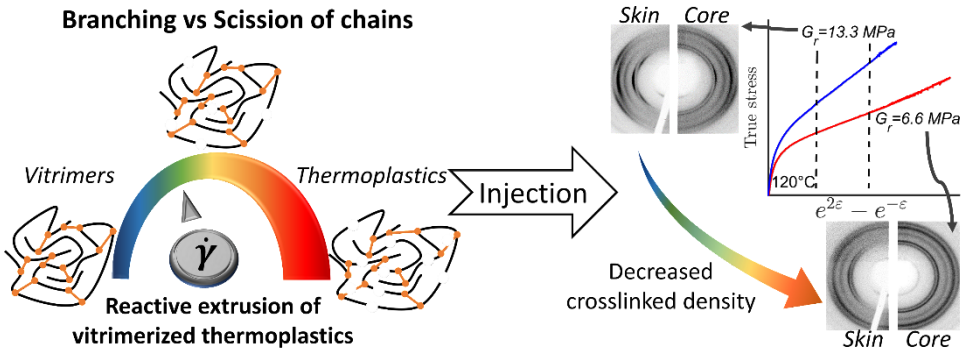

Key words: Vitrimer, continuous reactive extrusion, epoxy, process engineering

Abstract

This study examined the effects of continuous reactive extrusion on the properties of vitrimerized thermoplastics derived from polybutylene terephthalate (PBT). PBT formulations were prepared using epoxy (crosslinker) and zinc acetylacetonate (transesterification catalyst) to form dynamic covalent networks. Reactive extrusion was performed at different screw rotation speeds (50, 100, 200rpm) with controlled residence times to compare the effects of the shear stress during the formation of crosslinks on the vitrimer properties. The rheological behavior of the extruded vitrimerized PBT suggests that competition between chain scission and branching occurs during the dynamic crosslinking of thermoplastics. Increasing the shear stress and/or time in the extruder was found to favor chain scission over crosslinking which makes gelation unattainable. In the case of injection molded specimens, tensile and X-ray diffraction tests of vitrimerized PBT extruded at different shear stress indicated a significant relationship between the degree of crosslinking, the orientation of crystallites, and the ability of the polymer network to withstand deformation at elevated temperatures.

1. Introduction

Vitrimers represent a unique class of polymers that can undergo reversible structural modifications under specific conditions through associative dynamic exchange of covalent bonds.[1,2] These characteristics enable the self-healing, reprocessing, and reshaping of crosslinked polymers. The concept of vitrimers was first introduced by Leibler and Coll. in 2011 and has attracted considerable interest within the scientific community.[3] Initially, vitrimers were ester linked networks made from epoxy resin cured with dicarboxylic acids or acid anhydrides, enabling transesterification upon heating. Subsequent research has expanded this framework to include a variety of chemical reactions, such as transimination and transamination, thereby broadening the vitrimer toolkit.[4–9] A range of activation mechanisms, including heat, light, and electricity, have been used to trigger the covalent bond exchanges in these materials.[10–12] The process of vitrimerization, defined in this study as the incorporation of associative dynamic covalent bonds into a polymer matrix, was rapidly applied to thermoplastic matrices. Various commodity thermoplastics have been successfully vitrimerized through the incorporation of functional groups present along the polymer chain via grafting or copolymerization, or through chain extension reactions.[13–17]

Among thermoplastics, polybutylene terephthalate (PBT) is particularly suitable for studying the effect of vitrimerization because of the low reactivity of its hydroxyl end group, which minimizes the risk of undesirable side reactions (*e.g.,* epoxy-hydroxyl addition) during mixing and crosslinking.[15,18,19] PBT is commonly vitrimerized through the introduction of a crosslinker and a transesterification catalyst. These reactants are referred to as vitrimerizing agents in this work. The vitrimerization of PBT has been reported using methods such as reactive microcompounding[14,15,20] and solid-state crosslinking.[21] In previous studies,[15,16] reactive microcompounding was inaccurately conflated with reactive extrusion. However, they essentially differ, as the former is a discontinuous process and reactive extrusion is a continuous process. In reactive micro-compounding, the homogeneous melting and mixing of vitrimerizing agents with PBT is ensured by the presence of a recirculation channel, sending the reactive mixture back to the microcompounder screws. In continuous reactive extrusion (CRE), the screw profile and die are adjustable, allowing the conveying and mixing zones to be alternated. The conveying zones are used to transport solid and molten materials, such as the pristine polymer and its mixture with other products (reactive and/or fillers). In these zones, where the flow is laminar, there is very little mixing. To achieve homogenization of the extruded material, mixing zones comprising kneading blocks (often combined with a reverse-pitch element positioned downstream) are included. This reverse-pitch element ensures a 100% filling of the mixing zones. The specific geometry of the mixing elements in CRE generates a high local shear stress,[22] which may significantly influence the morphology and final properties of the polymers and their blends.[22,23]

The formation of dynamic crosslinks, which are indispensable for vitrimers formation, and the impact of shear rate during CRE on network formation are key areas of exploration. The formation of hydrogels[24] of microgels[25] under stress has been observed to impact their microstructure and subsequent properties, whereas competition between chain scission and branching have been reported for high density polyethylene during CRE.[26] Although the adoption of vitrimerized thermoplastics at larger scale requires the use of continuous manufacturing processes such as CRE, the effect of the operating conditions on the properties of vitrimers remains under-investigated. In a previous study, the feasibility of producing vitrimerized PBT by CRE was explored, maintaining a screw rotation speed of 60 rpm and a residence time of less than 5 mins.[20] This approach led to the concept of a 'pre-vitrimer,' where dynamic crosslinking occurs during a post-extrusion step[20] to limit the viscosification of the network and the potential risk of extrusion line plugging. Furthermore, a recent investigation indicated that PBT can experience significant thermal degradation during extrusion, even when exposed to an inert atmosphere.[27] Hence, it is crucial to ascertain whether vitrimerization is a suitable option for short extrusion residence times.

This study focuses on examining the influence of shear rate during continuous extrusion on the morphology and rheological properties of PBT 'pre-vitrimers,' obtained by adding 1.8 wt. % of diepoxide to PBT. The screw rotation speed was varied between 50, 100, and 200 rpm to create different shear rates during extrusion, which took place within a controlled timeframe. The rheological behavior and thermomechanical properties of the resulting materials were analyzed, and WAXS measurements of the injection-molded samples were performed to investigate the influence of the rheological properties on the specific microstructures that develop during material shaping.

2. Experimental section

2.1 Materials

Polybutylene terephthalate (PBT) Crastin® S600F40 NC010 (M_n = 47 kg.mol^{-1})[28] was purchased from DuPont. Before use, the PBT pellets were dried overnight at 120 °C. Zinc (II) acetylacetonate (Zn (II)), epoxy D.E.R 332 (epoxy equivalent

weight: 178 g.mol^{-1}), 1,1,2,2 tetrachloroethane, and Irganox 1010 (pentaerythritol tetrakis(3,5-di-tert-butyl-4-hydroxyhydrocinnamate)) were obtained from Merck. The Zn (II) catalyst is supplied as a powder that tends to aggregate during storage. To mitigate this issue, the powder was ground using a mortar and pestle, and dried in a vacuum oven overnight at 60°C. This process was performed to remove any adsorbed water from the powder surface.[29] The FTIR spectra of the Zn(II) powder both before and after drying (see Figure S1) revealed a decrease in the broad peak in the range of 3200–3600 cm^{-1}. It should be noted that all other chemicals used in this study were employed as received, without any modifications or alterations.

2.2 Sample preparation

2.2.1 Reactive solution (Epoxy, Zn (II) catalyst, and Irganox 1010)

To ensure uniform preparation, the catalyst and thermal stabilizer (Irganox 1010) were initially dissolved at 70°C in epoxy for 15 mins. Visible fumes were observed throughout the dissolution process, which were thought to result from the evaporation of small water molecules remaining in the powder materials. Upon successful dissolution, a transparent yellow solution was obtained and referred to as the 'reactive solution'. The reactive solution formulation was as follows: 100/20/10 (mass of epoxy/catalyst/Irganox 1010). The potential hydrolysis of the epoxy by hot water[30] was ruled out by comparing the FTIR spectrum of the reactive solution, as measured before and after dissolution, to the spectrum of the initial products (i.e., Zn(II), Epoxy DER 332, and Irganox 1010). The results of this comparison are shown in Figure S2.

2.2.2 Microcompounding (MC)

Reactive mixing

In a previous study[14,20], vitrimerized PBT samples that did not undergo the continuous extrusion process were prepared using procedures similar to those used in the present study: 10 g of PBT pellets were weighed and manually mixed with the corresponding amount of the reactive solution (0.234 g) for 3 mins. The sticky pellets were then inserted into the DSM Xplore twin-screw micro-compounder under a nitrogen flux equipped with a recirculation channel to control the residence time (2 min 30 s). Reference samples were prepared with three screw rotation speeds of: 50, 100, and 200 rpm, designated as Ref_{50nc}, Ref_{100nc}, and Ref_{200nc}, respectively. The operating parameters, along with the product proportions, are presented in Table 1, and Figure 1A, which also includes a schematic of the preparation process.

Injection-molding of samples prepared by MC

The samples were then injection molded into 60 mm × 25 mm × 2 mm plates at 270°C for the barrel and 60 °C for the mold. This was performed using a DSM Xplore Micro 12 cc injection-molding machine. At a screw rotation speed of 100 rpm, the reactive mixture was left in the microcompounder for up to 8 min before being injection molded into tensile and 40 mm × 10 mm × 4 mm DMA specimens.

2.2.3 Continuous reactive extrusion (CRE)

Reactive mixing

Vitrimerized PBT was prepared using a modular intermeshing co-rotating twin-screw extruder TSE 24 (Thermo Scientific™) with a screw diameter (D) of 24 mm and L/D ratio of 40 (where L is the length of the screw). The extruder was equipped with a volumetric feeder (K-Tron, K2-MV-T35) and feed hopper. The calibration of the PBT exiting the volumetric feeder was performed by weighing the amount of PBT at the exit of the feeder at various feeder screw rotation speeds, and a calibration curve was obtained, allowing for the control of the PBT feed rate by weight. Additionally, prior to all the experiments, the weight of the PBT fed to the extruder was controlled to ensure that the correct quantity was fed to the extruder. The extruder screw rotation speed was varied at 50, 100, and 200 rpm. The extruder screw profile is shown in Figure 1B. PBT pellets were fed through a conveying zone under nitrogen flow and then arrived in the mixing zone (composed of six orthogonal kneading blocks and a reverse pitch-element) which was maintained at 270°C to ensure complete PBT melting. It is important to note that for the experimental settings used in this work, the feed rates fell below the minimum recommended rate of 1.82 dm³/h as specified by the feeder manufacturer, equating to approximately 2.4 kg/h of PBT based on a density of 1.31 g/cm³ (source: campusplastic website). Although a calibration curve was used to control the feed rates during these conditions, and the feed rate was controlled before and after extrusion, this may have led to variability in the PBT feed rates, potentially affecting the material composition and properties. However, the impact of these possible variabilities on the overall conclusion of this study was deemed negligible; nonetheless, this point should be considered in studies requiring high formulation precision. The temperature of the extruder profile was set at 270°C to maintain parameters as close as possible to those used for the reference samples. A small amount of pristine PBT was extruded for 2 min 30 s at 100 rpm and is labelled "PBT_{extru}". For vitrimerization of PBT, the reactive solution (epoxy, Zn (II) catalyst, and Irganox 1010) was added using a syringe pump (KDS 100 LEGACY, 60 mL syringe) at a controlled flow rate (quantities in grams are given in Table S2) after the first mixing zone, which ensured melting of the pristine

PBT pellets. The melted PBT and reactive solution were then passed through five mixing zones before exiting the extruder die, cooled by nitrogen flow, and cut into pellets. The residence time after the injection of the reactive solution was determined using a colored tracer, and the PBT feed rate was adjusted according to the screw rotation speed to obtain two types of samples corresponding to 1) a short residence time (< 2 mins 30 s) and 2) a long residence time (> 8 mins) at each screw rotation speed, as indicated in Table 1.

A)

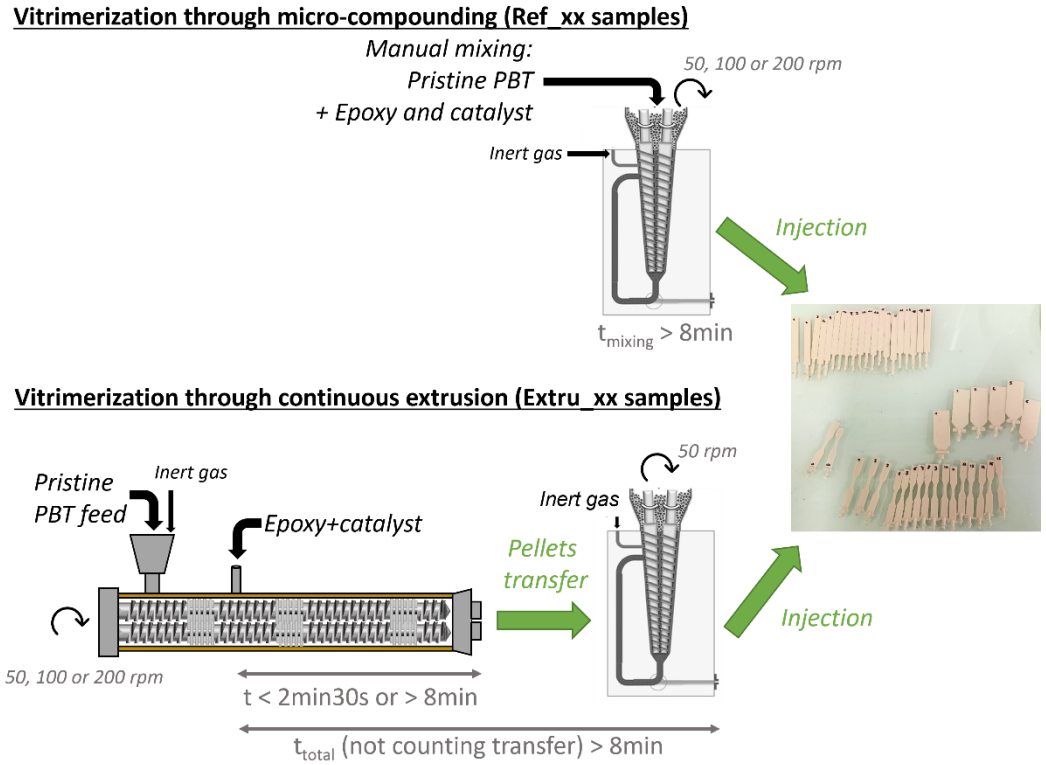

B)

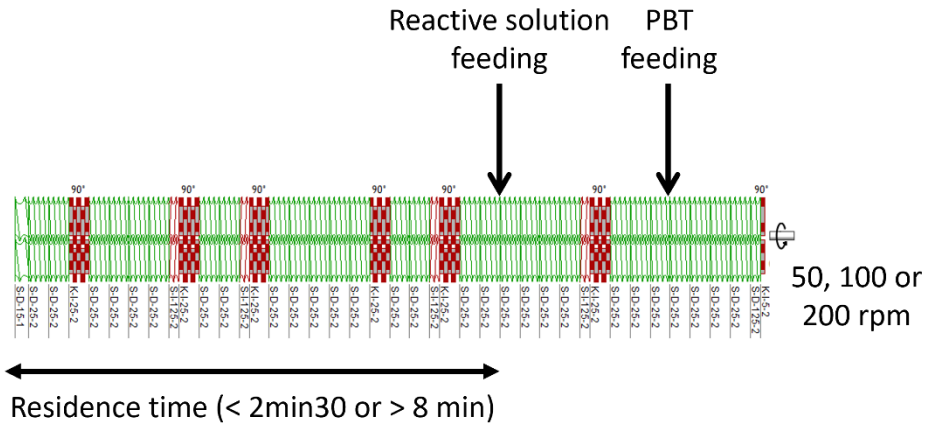

Figure 1 A) Schematic of the manufacturing process for the different samples of this study: Ref$_{xx}$ refers to samples only prepared in the micro-compounder, Extru_xx refers to samples prepared at different shear in the extruder then injection-molded.B) Extruder profile used for CRE of vitrimerized PBT. It comprised 5 mixing zones after feeding of the reactive solution; for these mixing zones, only the first, second and third were equipped with a reversed pitch element (from right to left)

Injection molding of samples prepared by CRE

Pellets obtained from continuous extrusion were injection molded with temperature similar to those described above (270°C for mixing in the DSM Xplore twin-screw microcompounder under nitrogen flow and 60°C in the mold). The use of the micro-compounder was an essential step in the process of melting the polymer, which was subsequently loaded into the injector barrel and injected into the corresponding molds for thermomechanical characterization tests. The pellets used in this process were prepared by extrusion the previous day and then stored in a sealed bag to minimize exposure to ambient air. Extruded formulations with short residence times (Extru_50, Extru_100, and Extru_200, as shown in Table 1) were left for a minimum of 5 mins in the micro-compounder at a screw rotation speed of 50 rpm to limit the impact of shear rate during this

experimental step and to complete dynamic crosslinking. This was performed in preparation for tensile testing and thermomechanical analysis (differential scanning calorimetry and dynamic mechanical analysis). Samples for rheology (Extru_50_{nc}, Extru_100_{nc}, and Extru_200_{nc}) were prepared without mixing for 5 min, melted within the twin-screw micro-compounder at 270°C for allowing injection-molding into a plate sample (60 mm x 25 mm x 2 mm) to measure the dynamic crosslinking of the extruded "pre-vitrimer" formulations. In the case involving the long residence time in the extruder (Extru_50_{long}, Extru_100_{long}, and Extru_200_{long}, table 1), the extruded pellets were also melted using the micro-compounder and injection-molded with the same temperatures.

*Table 1 Formulation and processing conditions of samples – for samples left a maximum of 2 min30 s in the extruder dynamic crosslinking was finished in micro-compounder at 50 rpm for 5 min before injection. *a small amount of Pristine PBT in these conditions for rheological and DSC measurements, labelled "PBT_{extru}". NA: non-applicable*

Process	Screws speed (rpm)	Residence time	Epoxy (wt. %)	Zn (II) (wt. %)	Irganox 1010 (wt. %)	Additional Mixing (50 rpm, MC)	label
Continuous Reactive Extrusion (CRE)	50	< 2 min 30 s	1.8	0.37	0.18	< 15 s	Extru_50_{nc}
						5 min	Extru_50
		> 8 min	1.8	0.37	0.18	< 15 s	Extru_50_{long}
	100	< 2 min 30 s	0	0	0.18	NA	PBT_{extru}
			1.8	0.37	0.18	< 15 s	Extru_100_{nc}
						5 min	Extru_100
		> 8 min	1.8	0.37	0.18	< 15s	Extru_100_{long}
	200	< 2 min 30 s	1.8	0.37	0.18	< 15 s	Extru_200_{nc}
						5 min	Extru_200
		> 8 min	1.8	0.37	0.18	< 15s	Extru_200_{long}
Micro-Compounding (MC)	50	< 2min 30 s	1.8	0.37	0.18	NA	Ref_{50nc}
	100	< 2min 30 s	1.8	0.37	0.18	NA	Ref_{100nc}
		> 8 min	1.8	0.37	0.18	NA	Ref_{100}
	200	< 2min 30 s	1.8	0.37	0.18	NA	Ref_{200nc}

2.2.4 Compression molding for X-ray diffraction samples

Samples for X-Ray diffraction were prepared using a Carver press (model 4120) from $Extru_{50nc}$, $Extru_{100nc}$, and PBT_{extru}. Rectangular samples (40 mm × 10 mm × 4 mm) were prepared by drying the pellets (80°C overnight under vacuum) of $Extru_{50nc}$, $Extru_{100nc}$, and PBT_{extru} and pressing them at 270°C in the mold for 10 mins. The samples were then cut into thin slices of 2 mm thickness for further analysis along the depth of the sample.

2.2.5 3D printing

The preparation of a filament (diameter 1.9 mm) for the 3D printing trials involved the use of well-dried Extru_100 pellets on a filament maker precision 3DEVO composer 450 extruder made up of four zones with adjustable temperatures. The temperature was set at 265°C in the first zone, where pellets were injected to ensure melting, and was gradually decreased in steps of 5°C to reach 250°C in the last heated zone, where the polymer exits. The fans were set between 8-10% power to cool the melted polymer and allow the formation of a filament with a regular diameter (1.7 mm ± 1 mm, > 1 m length). The use of the Extru_50 formulation did not allow the formation of a filament, resulting in the blocking of the equipment, whereas filaments made with Extru_200 formulation had an irregular diameter which hindered its use in 3D printing through fused filament fabrication (FFF).

3D printing was performed using a Raise3D Pro3 dual-filament printer, with the bed temperature was set at 85°C, and the 3D printing head was set at 270°C. The printing speed was set to 30mm/min with a layer thickness of 0.2 mm. The Extru_100 formulation was printed in the form of a hollow cube, a plain tensile specimen, and a Schwarz P ("primitive") surface to demonstrate the possibility of printing versatile shapes with the FFF technique (See ESI).

2.3 Sample characterization

2.3.1 Rheology

The rheological behavior of the samples was determined using an ARES G2 rotational rheometer equipped with a parallel plate geometry in a nitrogen atmosphere. Disk samples (diameter 20 mm, thickness 2mm) were cut from previously injection-molded plates samples (60mm x 25 mm x 2

mm). The disks were placed within a rheometer that had been preheated to 270°C. The geometry was then brought into contact, and the samples were allowed to melt for 15 s before the gap was reduced to 1.5 mm to ensure that proper contact was established between the two parallel geometries and samples during the measurement. To prevent edge effects, any excess melted material was quickly and carefully removed using a spatula before initiating the acquisition process. A low-amplitude oscillatory shear was applied at 270°C at a frequency of 1 rad/s and a strain of 0.5% with no normal force applied for 15 mins on a 1.5 mm thick sample to observe the dynamic crosslinking reaction after extrusion. Following this test, an angular frequency test with no normal force applied was conducted on the same samples from 240°C to 270°C at 5°C intervals ranging from 0.1 to 200 rad/s.

2.3.2 Swelling tests

To determine the gel fraction, 50 mg samples were immersed in 5mL of 1,1,2,2tetrachloroethane for 8 h at 120°C. If gels were present, they were separated from the solution and washed with chloroform for 24h. Subsequently, the samples were dried for 16h at 40°C, after which the residue was weighed. The gel fraction was determined as the ratio of the mass of the dried gel to the initial sample weight.

2.3.3 Thermal analysis

Dynamic mechanical analysis was carried out on a rectangular sample (40 mm x 10 mm x 4mm) in the tensile mode using a Metravib+300 analyzer under air atmosphere. The specimens were heated at a rate of 1°C.min^{-1} from room temperature to 250°C at a frequency of 1 Hz and a strain amplitude of 0.25 x 10^{-3}. DSC analyses were performed using a Mettler Toledo DSC 1 device under nitrogen atmosphere on samples weighing ~7-10 mg cut from an unused DMA specimen. An initial temperature ramp from -50°C to 250°C was used to erase the thermal history of the sample. The sample was then cooled to 50°C, followed by a second heating step to 270°C. The heating and cooling rates were set at 10°C.min^{-1}.

2.3.4 Mechanical testing

Tensile tests were conducted using a Bose 3000 tensile testing machine equipped with a thermal chamber. The primary objective of this study was to investigate the effect of extrusion on the characteristics of vitrimerized PBT. To minimize the impact of uncontrollable factors such as humidity and potential PBT degradation over time, all formulations were extruded and injection-molded on the same day. Consequently, we opted to produce a limited number of specimens, leading to only one specimen being tested at 20°C and 120°C per screw rotation speed instead of conducting a comprehensive statistical analysis. Nevertheless, the disparities in mechanical behavior that we observed at the two distinct temperatures were substantial enough to be deemed significant and consistent with the rest of the study's findings. The 'dog bone' shaped specimens (Figure S3) had a section S_o = 4 x 4 mm^2. They were specifically designed so that necking was always initiated in the center of the specimen, which ensures that the neck was always in the field of view of the cameras used for the strain measurement. The strain measurement was performed by 3D image correlation using the Aramis device provided by Gom®. To perform the image correlation, a random black speckle pattern was applied to the surface of the specimen using an airbrush. The measurement was conducted through a glass window placed on the front door of the temperature chamber. The relative speed of the testing machine's crosshead was 0.02 mm/s during the tests. The true longitudinal strain is defined as $\varepsilon = \ln(\ell/\ell_0)$ where ℓ_0 is a small length element taken in the specimen center along the tensile axis in the initial state, ℓ is the current size of this length element during the tensile test. The definition of the true transverse strain (ε_t) is the same, but for a length element taken along the specimen width. The nominal stress (σ_N) is given by $\sigma_N = F/S_0$, where F is the tensile force and S_0 the initial cross-section. The true stress (σ_V) is given by $\sigma_V = F/S$, where S is the actual cross-section. Assuming that the transverse strains in the width and thickness directions are equal, it can be checked that: $\sigma_V = \sigma_N e^{-2\varepsilon_t}$. Tensile testing was performed at two temperatures, 20°C and 120°C. Since the material was in a glassy state at 20°C, all samples were tested at the point of rupture. For tests carried out at 120°C, above the glass transition temperature of PBT ($T_g \approx$ 60°C), the materials did not exhibit brittle behavior and could undergo larger deformation. In this case, the tests were stopped when the upper limit of the testing machine for the relative crosshead displacement was reached (20 mm), with the exception of Ref_{100}, which ruptured before reaching the upper limit.

Creep experiments were performed on rectangular samples (50 x 10 x 4mm) with the Bose 3000 tensile equipment. A constant force (F = 164 N) was applied during 1 hour, and further recording was carried out 1 hour after unloading. A fluctuation of ±1N was observed during the loading phase.

2.3.5 X-Ray diffraction

Micro-diffraction measurements were then carried out on a home-made instrument,[31] which was equipped with a microfocus rotating anode (model Micromax 007HF, Rigaku), using Cu Kα radiation (λ = 0.154 nm) monochromatized by multilayer W/Si optics (FOX CU 2D 25_25P, Xenocs). The beam size was defined by a pinhole of 50 µm diameter, which was placed at the tip of the collimator at 4 mm in front of the sample. Two motorized translation stages (lateral and vertical moves)

with 1 µm step resolution enable the sample position in the X-ray microbeam to be precisely defined. X-ray diffraction signals were collected by an X-ray CCD camera (Quad-Ro:4096, Princeton Instruments) which was placed behind the sample.

The crystal dimensions were calculated from the (010) and (100) reflections of the PBT α-crystal form using the Scherrer equation:

$$S_{hkl} = \frac{K\lambda}{\beta_{hkl} cos\theta_{hkl}}$$

where S_{hkl} is the average crystal size along the dimensions perpendicular to the (hkl) plans. λ (1.54 Å) is the X-ray radiation wavelength, θ_{hkl} is the Bragg angle, and $\beta_{hkl} = \Delta(2\theta_{hkl})$ is the FWHM (Full Width at Half Maximum) of the diffraction peak. The Scherrer constant, denoted by K, is a value that is nearly equal to unity, although it depends on the morphology of the crystals, the nature of the crystalline lattice, and the Miller indices of the planes, as described by Langford.[32] Comparisons between Atomic Force Microscopy (AFM) observations and WAXS measurements revealed that the sizes estimated using the Scherrer formula do not correspond to the dimensions of the lamellae but rather to those of the crystalline blocks that make up the lamellae.[33,34] Additionally, the broadening of the peaks, which is a result of the measuring instruments, has not been taken into account. In most published works, where the Scherrer formula has been applied to semi-crystalline polymers, K is typically set at 0.9, and the same value was chosen in this work. It is important to recognize that the Scherrer formula is associated with numerous approximations; as such, the sizes provided by this formula should be considered as rough estimates and can only be used for comparative purposes. The detailed method of signal decomposition is given in the supporting information.

3. Results

3.1 Melt rheology

The evolution of G' and G" over time (Figure 2A) highlights the kinetics associated with the dynamic crosslinking process in the extruded vitrimer formulations (Extru_50_{nc}, Extru_100_{nc}, and Extru_200_{nc}) at 270°C. The conversion from PBT to vitrimerized PBT is achieved through a two-step mechanism. First, a chain extension reaction occurs with the diepoxy monomer, followed by the exchange of covalent bonds, which results in branching of the extended PBT chains between each other, ultimately leading to the formation of a three-dimensional (3D) dynamic crosslinked network.[15,20] Branching in thermoplastic polymers is commonly indicated by a significant increase in the melt storage modulus (G') while, the crossover point between G' and G'' indicates that the melt is transitioning from a viscoelastic liquid to a viscoelastic solid behavior. This crossover was used to determine the formation of the 3D dynamic crosslinked network through branching in previous vitrimers prepared from PBT.[14,20] Sample Extru_50_{nc} exhibited this crossover characteristic of dynamic crosslinking reactions (Figure 2A).[35] On the other hand, Sample Extru_100_{nc} did not display this feature, but there was a significant increase in G' from 75 Pa to 900 Pa. Yet, this highest value is nearly three times lower than the value measured at the end of the test for Extru_50_{nc} (2,675 Pa). This decrease in the final value of G' continued as the screw rotation speed increased. Extru_200_{nc} had a value of G' = 250 Pa and the difference between G' and G" (G' > G") was accentuated, indicating a decrease in the material's resistance to deformation.

The variables G' and G'' were also measured as a function of the angular frequency for the same samples used for the time sweep experiments. Measurements were performed from 240°C to 270°C in 5°C increments (raw data are shown in Figure S4a-c every 10°C). Figure 2B shows the G' and G'' values for the extruded formulations at the final test temperature of 270°C. In Figure 2B, Extru_50_{nc} exhibits dominant elasticity (G' > G''), which indicates a viscoelastic solid behavior. However, Extru_100_{nc} and Extru_200_{nc} both behave like viscoelastic liquids (G' < G''). At 250°C (Figure 2C), the Extru_100_{nc} sample displayed a unique feature, exhibiting G' and G'' nearly equal over the whole frequency range. Extru_200_{nc} did not exhibit this behavior; at any temperature (see Figure S4c), the loss modulus remained consistently higher than the storage modulus, similar to that of pristine PBT (as shown in Figures 2A, S5e, and S5f). The extrusion process did not induce any significant changes in the viscoelastic behavior (G'' > G' at any time, and similar slope with increasing frequency) of PBT_{extru} compared to its pristine form (see Figures S2d-e and S3e-f). However, it is important to note that the complex viscosity of PBT_{extru} was significantly reduced by a factor of approximately 4 at 270°C, and this difference increased with both time and temperature. This degradation is likely attributable to the previously reported thermal degradation,[36] caused by the high processing and testing temperature used in this study (270°C).

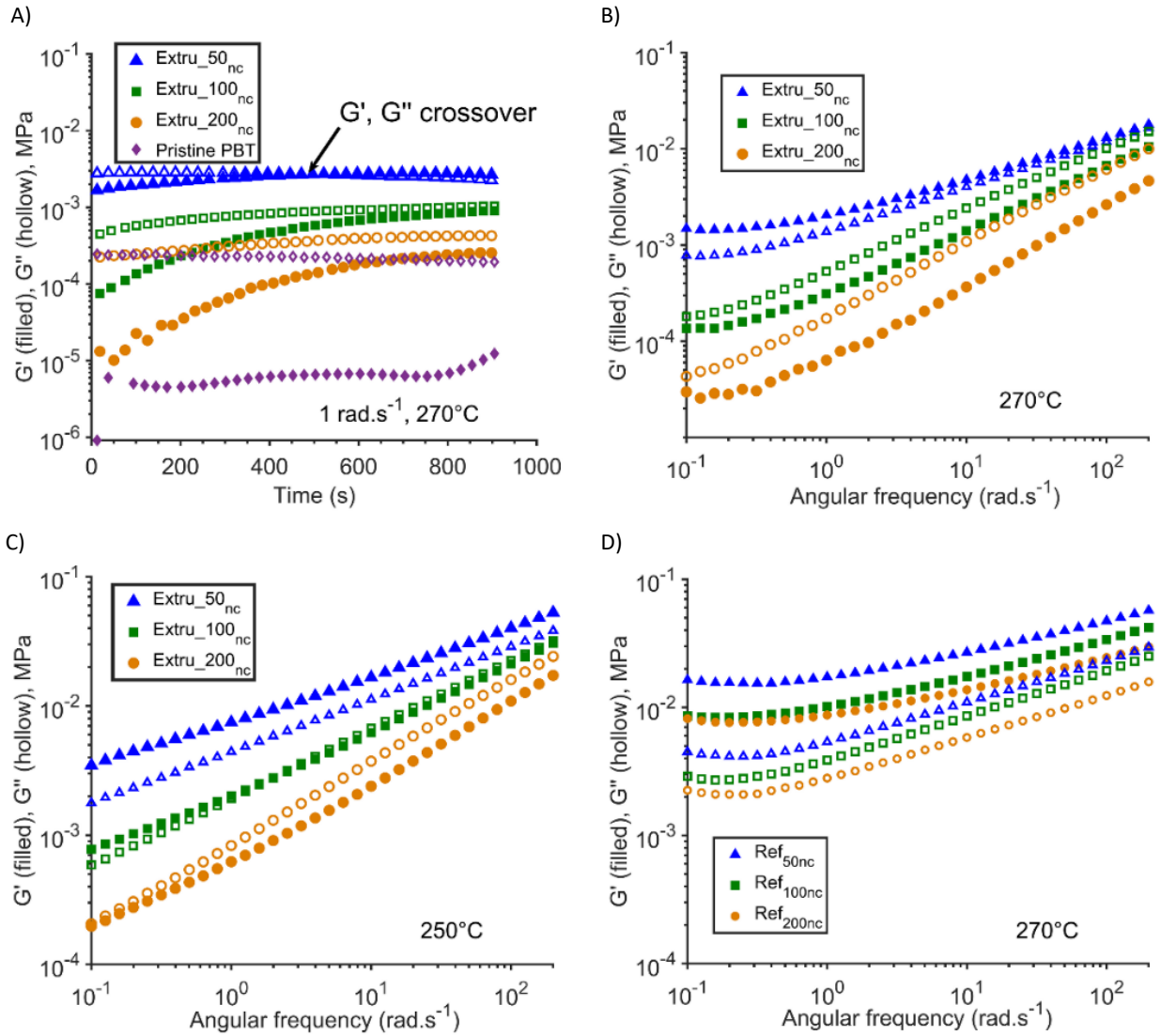

Figure 2 Filled symbols: storage modulus, hollow symbols: loss modulus: A) Dynamic crosslinking of Extru_50$_{nc}$, Extru_100$_{nc}$ and Extru_200$_{nc}$ at 270°C and 1 rad.s^{-1}, B) angular frequency test at 270°C for Extru_50$_{nc}$, Extru_100$_{nc}$ and Extru_200$_{nc}$, C) angular frequency test at 250°C for Extru_50$_{nc}$, Extru_100$_{nc}$ and Extru_200$_{nc}$, D) angular frequency test at 270°C for Ref$_{50nc}$, Ref$_{100nc}$, and Ref$_{200nc}$.

Similar behavior was observed for formulations with longer residence times (Extru_50$_{long}$, Extru_100$_{long}$, and Extru_200$_{long}$, as shown in Figure S5a-c). The modulus G' increased until it reached a plateau. Figures S5b and S3c show that the moduli G' and G'' were further reduced concomitantly with an increase in screw rotation speed. Starting with Extru_50$_{long}$, the rheological properties switched from a viscoelastic solid to a viscoelastic liquid behavior. However, the Extru_50$_{long}$ formulation still showed a crossover of G' and G'', indicating the formation of a crosslinked network. The results of extruded vitrimerized PBT formulations indicate that (i) increasing the screw rotation speed (and thereby the shear rate applied during vitrimerization) affects and limits the dynamic crosslinking, and (ii) a longer residence time at similar shear forces tends to decrease the viscoelastic properties (G', G'' and complex viscosity) of the materials.

Rheological measurements were performed on reference samples prepared using micro-compounding (ref$_{50nc}$, ref$_{100nc}$, and ref$_{200nc}$), and the results are reported in Figures 2D and S3d. A minor decrease in G'' was observed at higher screw rotation speeds. However, all the formulations were well crosslinked with G' > G'' at any frequency. These results highlight the difference originating from the operating conditions between microcompounding and continuous reactive extrusion, emphasizing a limiting factor for the processing of these materials.

To focus on the effect of the continuous extrusion process, Ref$_{100}$, Extru_50, Extru_100, and Extru_200 samples were selected for further analysis. The samples extruded with longer residence times exhibited a similar behavior to those extruded with shorter residence times. For the samples prepared using the microcompounder, the lack of meaningful differences for materials synthesized at 50, 100, and 200 rpm led us to focus on Ref$_{100}$.

3.2 Thermal analysis

3.2.1 Differential scanning calorimetry (DSC)

The thermal analysis of the samples is illustrated in Figure 3. DSC measurements of the second heating ramp between 200°C and 240°C are depicted in Figure 3A while Figure S6a-e displays the second heating cycle with area of integration used to calculate crystallinity. Upon vitrimerization, an increase in the melting temperature of PBT was observed (from 218°C for pristine PBT to 226°C for Ref_{100}). The melting temperatures (peak maximum in Figure S6) were comparable for Extru_50 and Ref_{100} (226°C and 225°C, respectively) and for Pristine PBT and PBT_{extru} (218°C and 219°C respectively, as shown in Figure S6f). Increasing the screw rotation speed slightly decreased the T_m from 226°C to 224° and 223°C for Extru_100 and Extru_200, respectively. The shape of the peak changed; pristine and PBT_{extru} exhibited two peaks associated with the first melting of small crystals, followed by the general melting of PBT crystals.[37] In the case of the vitrimerized PBT Ref_{100} and Extru_50, this double peak disappeared, resulting in a broadened single peak. In the case of Extru_100 and Extru_200, a double peak reappeared, while maintaining a higher melting temperature than unmodified PBT. The degree of crystallization of the samples was calculated using Equation 1:

$$X_c = \frac{\Delta H_{sample}}{\Delta H_\infty} \, x \, 100 \qquad (1)$$

Where X_c is the degree of crystallization, ΔH_{sample} is the enthalpy of melting, and ΔH_∞ is the enthalpy of 100% crystalline PBT (140 $J.g^{-1}$).[15,38] Numerical values for T_m, X_c, and ΔH_{sample} are given in *Table* ***2***, with the measurements shown in Figure S6a-f. A decrease in 2% of pristine PBT crystallinity is observed when vitrimerization occurred in the micro-compounder (Ref_{100}), while the extruded PBT and vitrimerized PBT showed a degree of crystallinity between 4 to 9% lower than the microcompounded formulations. The extruded vitrimerized samples show a slightly lower degree of crystallization than PBT_{extru} while evolving non-monotonically with the screw rotation speeds.

Table 2 Measurement by DSC: Maximum melting temperature T_m, Enthalpy ΔH, and crystallinity X_c calculated with $\Delta H_{100\%}$ = 140 $J.g^{-1}$ and integral between 100°C and 245°C.

Sample	Pristine PBT	Ref_{100}	PBT_{extru}	Extru_50	Extru_100	Extru_200
T_m (°C)	218	225	219	226	224	223
ΔH ($W.g^{-1}$)	61	58	54	51	53	49
X_c (%)	43	41	39	37	38	35

3.2.2 Dynamical mechanical analysis (DMA)

As depicted in Figure 3B, DMA measurements between 210°C and 240°C for the vitrimerized PBT samples showed a plateau at 240°C. Ref_{100} exhibited the highest storage modulus E' at 240°C (600 kPa) followed by Extru_50 (500 kPa). Extru_100 showed a rubbery plateau that was five times lower than that of Extru_50, with a G' value of approximately 100 kPa while Extru_200 showed a plateau at approximately 15 kPa, *i.e.,* just at the sensitivity limit of the machine. A rubbery plateau in the melt storage modulus (G') of thermoplastics owing to chain entanglements has been previously reported.[39] However, to the best of our knowledge, no experiments using DMA have reported such features. The G' value (E'≈3G'), as measured by rheometry in the molten state, was less than 10 Pa (as shown in Figure 2A). As a result, the absence of a plateau in the PBT storage modulus curve above the melting temperature is likely due to the resolution limit of the DMA measurement for E' (250 Pa). Furthermore, in DMA, an increase in entanglement leads to a longer rubbery plateau before abruptly dropping,[40,41] which is the opposite of the situation depicted in Figure 3B. Although this phenomenon may have been caused by a decrease in the crystallinity percentage of the vitrimerized formulation, it suggests that dynamic crosslinking of the network occurred for any processing parameter, despite the extruded polymers exhibiting progressively more thermoplastic behavior as the extrusion screw rotation speed increased (as indicated by the DSC data).

A)

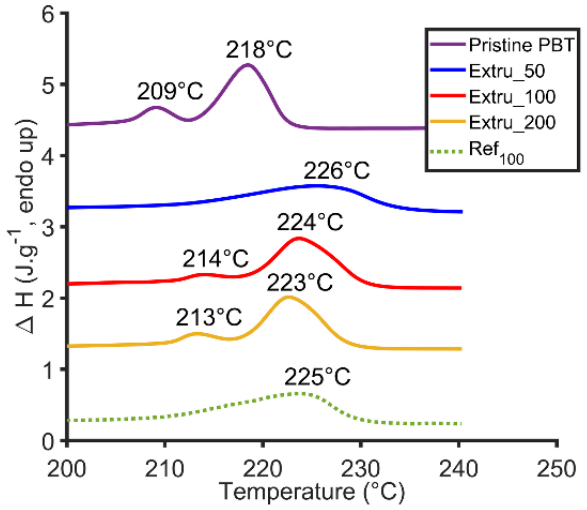

B)

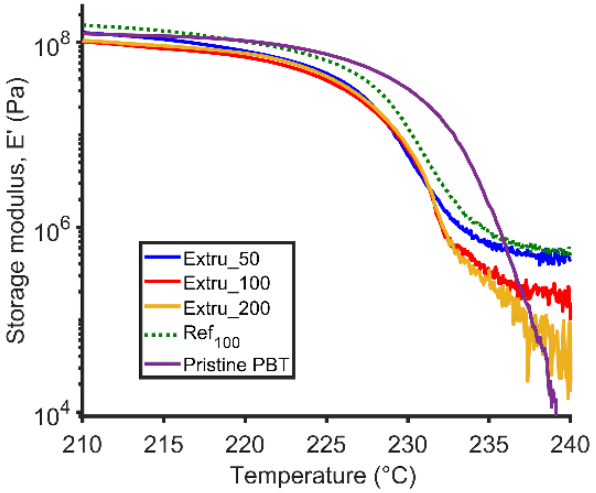

Figure 3 (Color online) A) DSC thermogram (second heating cycle), B) storage modulus of sample from DMA measurements

3.2.3 Swelling

The swelling results are shown in *Table* ***3***. Only the Extru_50 sample showed the formation of a gel, whereas Extru_100 and Extru_200 were completely dissolved. This suggests that although some degree of crosslinking was observed in the Extru_100 and Extru_200 samples, as indicated by the rheology and DMA data, the formation of an infinite 3D network, or gel, was not be possible.

Table 3 Gel fraction calculated from swelling tests on Ref_{100}, Extru_50, Extru_100, and Extru_200

Sample	Ref_{100}	Extru_50	Extru_100	Extru_200
Gel fraction (%)	45%	38%	x	x

3.3 Mechanical testing

3.3.1 Tensile testing

The nominal stress-true strain curves ($\sigma_N(\varepsilon)$) for Extru_50, Extru_100, Extru_200, pristine PBT, and Ref_{100}, measured at room temperature (below T_g, Figure 4A) and 120° (above T_g, Figure 4B), are depicted in Figure 4. The corresponding true stress-true strain curves ($\sigma_V(\varepsilon)$) are shown in Figure S7. Tables 4 presents the Young's moduli (E), yield stresses (σ_y), and yield strains (ε_y) for each material, as determined from the stress-strain curves (see Figure 4). At 120°, the yield stresses and strains could not be measured for Extru_50 and Ref_{100}, owing to the absence of a 'necking' behavior in their corresponding nominal stress-true strain curves.[14,20] The strains and stresses at rupture ((σ_R, and ε_R) for the specimens that failed during the test are also provided in Table 4, as shown in Figure 4A.

A)

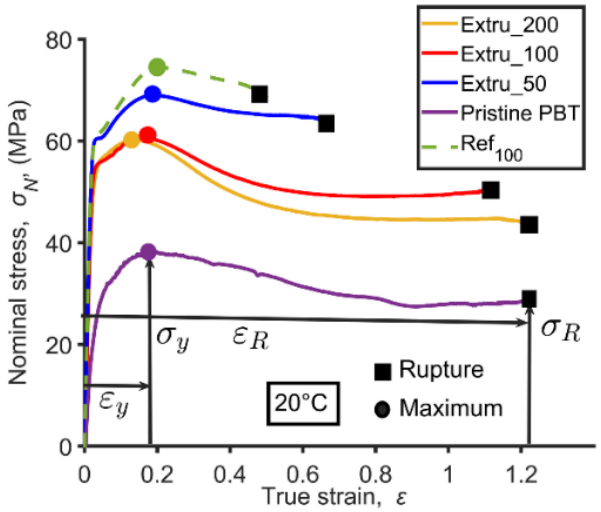

B)

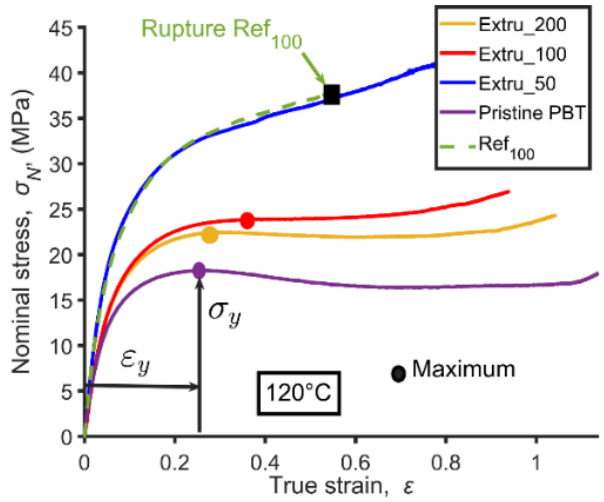

Figure 4 (Color online) Nominal stress-True strain curves A) $\sigma_N(\varepsilon)$ curves measured at room temperature $\sigma_V(\varepsilon)$ curves measured at 120°C

Table 4 Tensile property measurements at room temperature (20°C) and 120°C. N/A: Not Applicable, "-" indicates that these values were above the upper limit of the measurement set-up used in this (> 20 mm), see section 2.3.4 for details.

		Pristine PBT	Extru_200	Extru_100	Extru_50	Ref_{100}
E (MPa)	20°C	2300	2600	3000	3200	3200
	120°C	332	357	374	538	522
σ_y (MPa)	20°C	38	60	61	69	74
	120°C	NM	22	24	N/A	N/A
ε_y	20°C	0.19	0.15	0.16	0.19	0.20
	120°C	NM	0.29	0.4	N/A	N/A
σ_R	20°C	29	44	51	64	68
	120°C	-	-	-	-	37.6
ε_R	20°C	1.23	1.20	1.13	0.67	0.5
	120°C	-	-	-	-	0.6
G_r	120°C	3.8	5.3	6.6	13.3	14.2

The mechanical properties (E, σ_y and σ_R) of the vitrimerized materials (Extru_50, Extru_100, Extru_200, and Ref_{100}) were found to be superior to those of pristine PBT at room temperature. Furthermore, the effect of the extruder screw rotation speed on the mechanical properties was clearly demonstrated, with the stress, Young's modulus, yield stress, and stress at rupture being higher at lower screw rotation speeds. At the lowest screw rotation speed (Extru_50), the tensile behavior was comparable to that of the reference vitrimer (Ref_{100}). Additionally, it was observed that the smaller the σ_R value, the larger was the strain at rupture (ε_R). The results from the experiments conducted at room temperature (Figure 4A, Table 4) were applicable to those conducted at 120°C (Figure 4B, Table 4), except that measurements for σ_y, ε_y, σ_R, and ε_R could not be obtained at 120°C.

In the plastic regime (above a threshold value of $\varepsilon = 0.3$), the extruder screw speed had a significant effect on the strain hardening for measurements conducted above the glass transition temperature (120°C). The slope of the stress-true strain curves was greater when the screw speed was lower, as evidenced by the Haward-Thackray plot in Fig S6.[42] The Haward-Thackray model assumes that the Gaussian chain approximation can be used for describing the stretching of the macromolecular network during plastic flow. To use the Haward-Tackray model, it is necessary to assume an isochoric deformation process. This assumption seems valid in the present case, as the absence of whitening shows that the polymer does not cavitate. Moreover, the stress-induced α → β transition leads to only very limited density changes as it is detailed in the supporting information of a recent paper.[43] Beyond the yield point, the variations of the true stress ($\Delta\sigma_v$) can then be described using a rubber elasticity spring: $\Delta\sigma_v = G_r\left(e^{2\varepsilon} - e^{-\varepsilon}\right)$, where G_r is the strain hardening modulus. The strain-hardening modulus, G_r, can be calculated using this method (see Table 4). As expected, pristine non-crosslinked PBT exhibited the lowest G_r value. Furthermore, the effect of the extruder screw rotation speed on strain hardening was confirmed as slower screw rotation speeds resulted in higher G_r values.

In conclusion, increasing the screw speed in the extruder reduces the mechanical performance of the extruded polymers, as evidenced by a decrease in Young's modulus, strain hardening modulus, yield stress, and stress at break.

3.3.2 Creep experiment

The creep behavior of the extruded formulations and pristine PBT at 160°C, 180°C and 200°C are depicted in Figure S9a-d. Figure 5 depicts the creep rate and creep strain, while Figure S9e-f illustrates the instantaneous strain recovery and permanent strain calculated following the schematic shown in Figure S10. Pristine PBT exhibited the highest flowability under the applied load. Furthermore, it was found that creep resistance, in terms of rate, strain and permanent deformation, increased with a decrease in the shear forces applied during vitrimerization. However, there is no specific trend associated to the extrusion flow rate for instantaneous recovery. Notably, at 160°C, the vitrimerized formulations recovered less when the load was removed.

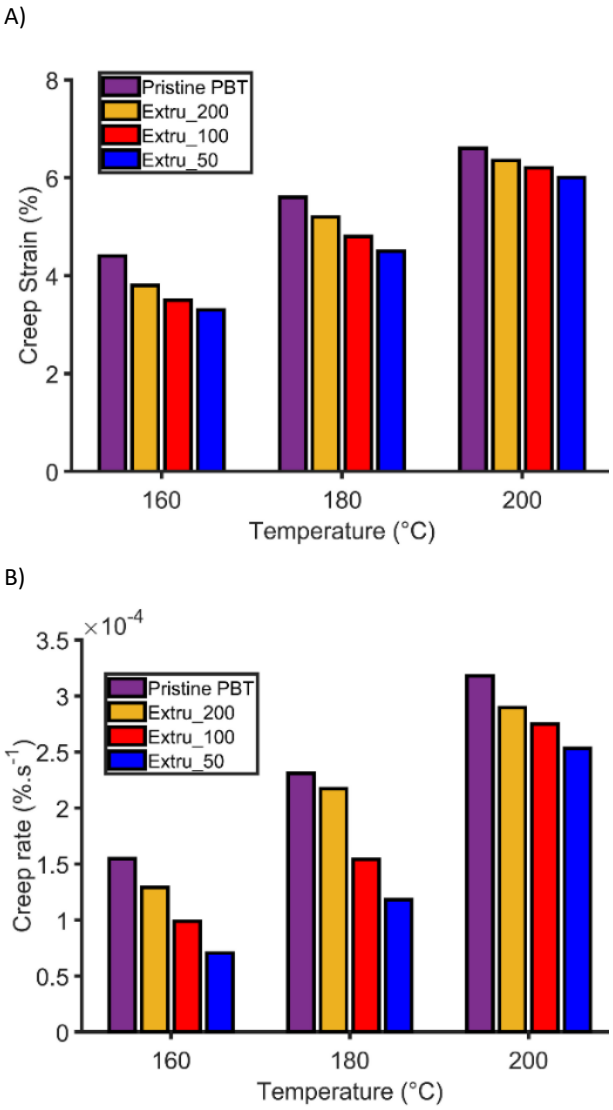

Figure 5 (Color online) Creep results (constant applied force: 167 N for 1h) of extruded PBT and vitrimerized PBT: A) creep rate, B), creep strain.

3.4 WAXS

The injection molding stage is prone to cause polymer orientation.[44,45] During this stage, the velocity profile ($v(x)$) of the polymer along the mold thickness is approximately parabolic, For unidirectional flow (Figure 6A), the shear strain rate is given by $\dot{\gamma} = \frac{\partial v}{\partial x}$. The shear stress is expressed by Equation 2:

$$\tau = \eta\dot{\gamma} \qquad (2)$$

Where the shear strain rate $\dot{\gamma}(x)$ and stress $\tau(x)$ vary linearly (Figure 6A) with the maximum values in the skin regions (near the mold walls) and minimum values in the core, the shear stress τ is oriented along the flow direction., This can result in polymer chain orientation in the direction of flow near the skin, leading to the development of an oriented microstructure known as "shish-kebab" morphology during the solidification/crystallization stage.[44,45]

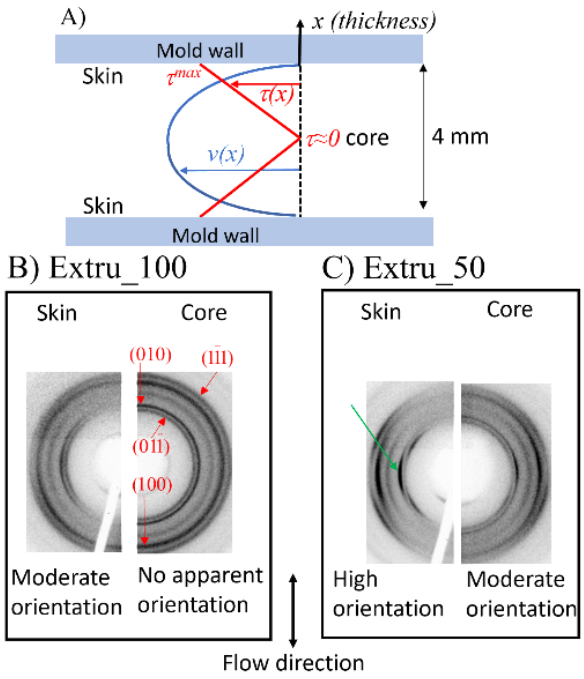

Figure 6 Polymer orientation during injection molding: a) Schematic representation of the velocity and shear stress profiles along the specimen thickness during injection molding, b) WAXS patterns measured in the skin and in the core regions for Extru_100 and c) WAXS patterns measured in the skin and in the core regions for Extru_50. The indexation corresponding to the 4 more intense reflections is also indicated in the left pattern (figure 6B)

WAXS measurements were performed along the specimen thickness, and the patterns obtained in the core and skin regions are shown in Figure 6B and 6C for the Extru_50 and Extru_100 samples, respectively. To take advantage of the patterns' symmetry, only half of the diffraction rings are shown. For the Extru_100 sample, the intensity was uniform along the diffraction rings in the measurements obtained from the specimen core, indicating an isotropic crystalline microstructure. However, in the skin region where the shear stress was higher, the intensity was not uniformly distributed along the rings, indicating that the polymer crystallites were oriented in this area. In contrast, the intensity of the Extru_50 sample was highly concentrated in certain parts of the diffraction rings, indicating a more pronounced polymer crystallite orientation in the skin region compared to that of the Extru_100 sample. The microstructure of the Extru_50 sample is moderately oriented in the core region. Therefore, to eliminate the influence of the injection process (anisotropy), vitrimerized PBT samples ($Extru\_50_{nc}$ and $Extru\_100_{nc}$) and a PBT_{extru} sample prepared by compression molding were used for the crystal size measurements. The resulting WAXS patterns measured along the specimen thickness show that crystallization occurred in an isotropic manner for both vitrimerized materials (see Figures S9).

The intensity profile versus 2θ (θ: diffraction angle) and the decomposed peaks are shown in Figure 7 for $Extru\_50_{nc}$ and

in Figure S11 for the other formulations. The decomposition procedure is detailed and illustrated in the SI (Figure S12). In Figure 7, the normalized intensities of the (010) and (100) lattice planes of both materials are presented in the same plot. The Extru_100 sample exhibited broader peaks than those of Extru_50_{nc}. As can be deduced from the Scherrer formula, the broader the peaks, the smaller the crystal dimensions. The crystal dimensions along the direction perpendicular to the (010) and (100) planes are listed in Table 5. Peak broadening was observed in all Extru_100_{nc} peaks of the raw signal and their fitting (Figure S13) compared to Extru_50_{nc}. Upon comparison with the PBT_{extru} signals (Figure S13), the (010) lattice plane peak of Extru_50_{nc} did not show any particular change, whereas the (100) peak was broader. The (010) lattice plane diffraction peak of Extru_100_{nc} was sharper than that of PBT_{extru}, whereas the (100) diffraction peak almost perfectly fitted the PBT_{extru} signal.

A)

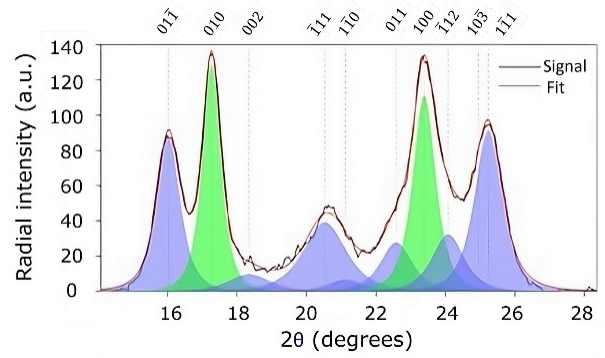

B)

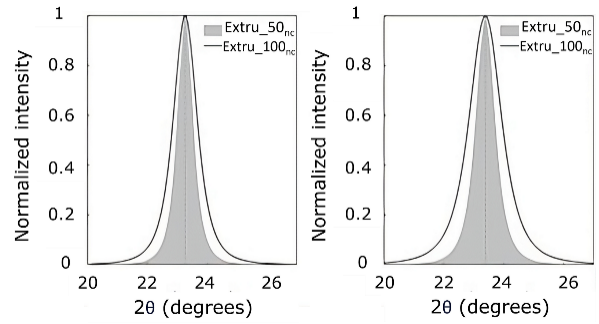

Figure 7 WAXS measurements for material A: Measured intensity profiles, fitted intensity profiles and decomposed peaks. Peak broadening at high extrusion speed. (010) and (100) reflections for Extru_50_{nc} and Extru_100_{nc}.

Table 5 Crystal sizes calculated using the Scherrer method for Extru_50 and Extru_100 samples

	hkl Miller Indices	
	(010)	(100)
PBT_{extru}	11 nm	6nm
Extru_50_{nc}	13 nm	10 nm
Extru_100_{nc}	9 nm	6 nm

In Figure S14, we show the X-ray intensity profiles measured along the (010) ring (see ring indexation in Figure 6B). The normal vector of the corresponding planes is perpendicular to the chain average direction in crystals (c axis of the triclinic cell).[46] Using these profiles, we calculated the Hermans orientation parameters[47] (f_{010}) associated with the (010) reflection. When the polymer chains in the crystals were randomly distributed, this parameter was zero. When the chains were oriented along the flow direction, f_{010} tends towards -0.5. The normal vector associated with the (010) planes is then situated in a plane perpendicular to the flow direction and, on the WAXS pattern, the X-ray intensity corresponding to this reflection becomes concentrated along the equatorial axis (see the green arrow in Figure 6C). In the case of Extru_100, we obtained f_{010}=-0.02 (≈0) in the specimen core and f_{010}=-0.10 in the specimen skin. For Extru_50, the core and skin values are -0.09 and -0.2 respectively.

The results of XRD analysis show that crosslinking in PBT leads to the formation of a core-shell structure in injection-molded parts, which likely affects the mechanical properties in unidirectional tensile loading. As the crosslinking density is reduced, this orientation effect decreases, suggesting a direct relationship between crosslinking degree and the structural orientation within the PBT matrix. Further analysis reveals that a high degree of crosslinking, corresponding to a solid-like viscoelastic behavior in the melt, results in crystals of larger average size. Conversely, when the crosslinking is less pronounced, resulting in a liquid-like viscoelastic behavior of the melt, the crystals tend to be closer in size to those found in unmodified PBT. This indicates that the crosslinking density not only affects the macroscopic mechanical properties but also has a profound effect on the microstructural level, influencing crystal size and distribution within the polymer.

4. Discussion

The extrusion process and operating conditions significantly impacted the properties of the vitrimerized PBT. A higher shear intensity (controlled by screw rotation speed in this study) led to an impossibility to achieve effective crosslinking in vitrimerized PBT prepared with the same amount of vitrimerizing agent. Gelation is typically indicative of successful vitrimerization in thermoplastics.[13,15,20,48] This is particularly true when a diepoxy monomer is used as a vitrimerizing agent. The epoxy reacts via polyaddition with PBT end-chain carboxyl groups to produce hydroxyesters, and crosslinking can occur through transesterification between one hydroxyester (resulting from epoxy-carboxyl polyaddition) and a free hydroxyl group.[49] When the PBT was vitrimerized through microcompounding or extruded at 50 rpm using CRE (Extru_50), effective crosslinking and gel formation were achieved, confirming that these formulations

were vitrimerized through dynamic crosslinking. This leads to the question for materials extruded at 100 and 200 rpm. Time sweep measurements of Extru_100$_{nc}$ and Extru_200$_{nc}$ (Figure 2A) showed signs of increasing G' modulus, which is typical of branching reactions.[15,26,50] However, gelation (the formation of a gel with infinite molar mass) was not attainable for these samples extruded at higher shear stress. The DMA plateau values for different samples at 240°C are given in Table 6, along with the average molecular weight M_c between crosslinks, calculated from the theory of rubber elasticity ($M_c = \frac{3RTd}{E'_{rubbery}}$ where R is the universal gas constant, T is the absolute temperature in Kelvin and d = 1110 kg.m^{-3} the melt density of PBT taken from the manufacturer's data, source: campusplastics website)[51–53]. The crosslink density was then calculated by $\nu_c = \frac{M_{PBT}}{M_c}$, with M_{PBT} = 47 kg.mol^{-1}.[28] The crosslinking densities of Ref$_{100}$ and Extru_50 were respectively 2 and 1.65, whereas the crosslinking density of Extru_100 was 0.36 (five time lower). The crosslinking density of Extru_200 was 0.05. Only Ref$_{100}$ and Extru_50 had a crosslinking density greater than 1, indicating that all PBT chains were connected to at least one diepoxy molecule and could form an infinite gel. Considering that, in presence of a transesterification catalyst, the equivalent molecular weight of epoxy is M_{epoxy}/4 = 89 g.mol^{-1} (as the diepoxy is tetrafunctional is these conditions). On the other hand, the PBT has an average functionality comprised between 1 and 2 (as the PBT chain can be terminated by either a COOH and a OH group or by two COOH groups)[54,55]. This means that the theoretical weight ratio of PBT to epoxy to get $\nu_e = \frac{M_{eew\_PBT}}{M_{eew\_epoxy}} = 1$ is comprised between 264:1 (for M_{eew_PBT} = 23.5 kg.mol^{-1} and $M_{eew\text{-}epoxy}$= 89 g.mol^{-1}) and 528:1 (for M_{eew_PBT} = 47 kg.mol^{-1} and $M_{eew\text{-}epoxy}$= 89 g.mol^{-1}).

Table 6 Elastic modulus E' at 240°C from DMA measurement, ν_c: the crosslink density

	Ref$_{100}$	Extru_50	Extru_100	Extru_200
E (kPa) @240°C	613	500	108	15
M_c (kg.mol^{-1})	23	28	132	947
ν_c	2	1.65	0.36	0.05

In this study, the weight ratio was fixed at 54:1. This represents a high excess of epoxy compared with the theoretical minimum required to form a 3D network. The maximum ν_c value obtained was 2 (Ref$_{100}$ sample) which would correspond, in the case of a 100% conversion without production of by-products and secondary reactions or chain scissions, to a weight ratio PBT to epoxy of 258:1 (with M_{PBT} = 47 kg.mol^{-1}). This value was lower when the material was extruded at a higher screw rotation speed. The ν_c values calculated from E' for Extru_50, Extru_100, and Extru_200 would correspond to a weight ratio respectively of 315:1, 1,483:1, and 10,640:1 (with M_{PBT} = 47 kg.mol^{-1}). The decrease in the measured ν_c value during the extrusion process, despite the initial proportion of epoxy being held constant, raises questions on how the crosslink density is affected by the extrusion process.

As mentioned earlier, the geometry of the mixing zone in continuous extrusion can induce high local shear rates. This is useful to ensure the homogeneity of the extruded product, but this type of process is only well suited to thermoplastics or materials able to flow like viscoelastic liquids. Vitrimers, by definition, are crosslinked materials and therefore do not follow viscoelastic liquid behavior, behaving instead like viscoelastic solid materials.[3,56–58] In this study, the rheological results (Figure 2) demonstrate this point. Vitrimerization greatly increases the melt viscosity through branching and generates higher shear stresses; if the shear rate increases as well (higher screw rotation speed), this leads to shear-induced chain scissions.[26] The gelation of the vitrimer is then hindered by the high level of scissions, a phenomenon similar to the way in which shear forces can limit gelation or change the morphology of hydrogels[24] and change the microstructure of microgels.[25] In the context of continuous reactive extrusion, this phenomenon has been described for the branching of high-density polyethylene.[26] Competition between branching and shear-induced chain scission has been reported, with chain scission becoming predominant at high molecular mobility (high temperature, high shear rate, and low molecular mass). This was indeed what occurred in our case - at 50 rpm, the shear intensity was not high enough for shear-induced chain scission to become prevalent. The PBT chains extended with the diepoxy monomers, and branching occurred through transesterification with limited chain scission through the extrusion line until the die. At higher screws rotation speed, the shear intensity was greater, causing chain scission to become predominant (Extru_100 and Extru_200).

Some other degradation mechanisms are possible, such as the thermal degradation of PBT, its hydrolysis and the formation of irreversible bonds through secondary reactions (through hydroxyl-epoxy addition or epoxy homopolymerization).[15,35,49,59] Thermal degradation in PBT or its hydrolysis during the extrusion process could lead to the formation of more carboxyl groups[18,27,54] which could participate in transesterification reaction to form a vitrimer. Moreover, all vitrimerized samples were mixed at 270°C during a similar period of time. Hence, thermal degradation or hydrolysis between vitrimerized samples are likely equivalent, therefore differences in Extru_50, Extru_100 and Extru_200 are due to the different shear intensities applied during extrusion.

As the number of scissions increases due to the shear stress, the PBT molecular weight decreases concomitantly. Thus, with shorter chains, a higher epoxy to PBT ratio would be required. However, in this study, even with the initial presence of epoxy excess (~ 10 times higher), shear-induced chain scissions led to materials not being able to form a gel when the screw rotation speed was fixed at 100 or 200 rpm. Excess of epoxy has been reported to homopolymerized in vitrimer formulation leading to the formation of ether bond.[49,59,60] This is likely what occurs during the extrusion process at 270°C, after polyaddition between PBT carboxyl group and oxirane, the excess of epoxy forms short ether molecules through homopolymerization in all the samples presented in this study (Ref_{100}, Extru_50, etc.). This reaction makes further crosslinking impossible once a high level of shear scission occurred.

Samples extruded for a longer residence time ($Extru\_xx_{long}$, Figure S5a) showed signs of thermal degradation, as the moduli were lower compared to formulations with short residence times (Figure 2A). Thermal degradation is unlikely to be a determining factor for the effective crosslinking of the vitrimer if the residence is limited to 8 min as it is the case in this study as samples $Extru\_50_{long}$ shows also a viscoelastic solid behavior.

The increase in G' for samples prepared with long residence time ($Extru\_xx_{long}$) was unexpected, as it was reported that dynamic crosslinking of similar formulations was achieved in approximately 8 mins.[15,20] It is likely that during extrusion, the polymer broke at random locations along the chains, either on the hydroxyester bonds or on the PBT chains. However, when the temperature is reapplied at a low deformation rate, vitrimer bonds can (re)form through transesterification, which leads to an important increase in the moduli (by at least one order of magnitude) and the plateau after the melting of PBT crystals (Figure 3B). On the other hand, PBT chains cannot be repaired, so the gelation can no longer occur. This leads to a transition from a single infinitely connected gel (Ref_{100} or Extru_50), to a final polymer composed of a large number of finite vitrimer microgels that are not connected to each other (Extru_100 and Extru_200).

The changes in the melting temperature from the DSC data are similar to those reported in ref [15] for similar amounts of vitrimerizing agents.[15] However, the degree of crystallization was lower at all screw rotation speeds than that of PBT_{extru}. The results comparing PBT_{extru} to Pristine PBT (Table 3), indicate that the CRE process does decreases the degree of crystallization of PBT probably by thermal and/or hydrolytic degradation and even at short extrusion times.[61] For vitrimerized PBT, branching and crosslinking increase the thermal stability of the network (increase in melting temperature) while limiting regular packing of the polymer chains during cooling (decrease in the degree of crystallization). The transition from a double peak in PBT to a single broader peak in Extru_50, followed by a double peak for Extru_100 and Extru_200, can be combined with the increase in the size of the granular crystal layer perpendicular to the (010) planes followed by its decrease. As explained in the experimental section, the calculated size represents the average size that is useful for qualitative comparison. When crosslinking is effective (Extru_50), the formation of smaller crystallites is likely to be hindered, which increases the overall measured size crystalline blocks that make up the lamellae. Once the molecular mobility is increased by decreasing the crosslinking density, smaller crystallites might reform, again displaying the double peak characteristic of PBT. Also, the average crystalline blocks measured approximately return to the value measured for PBT (Table 5).

Creep experiments also confirmed that branching occurred in samples Extru_100 and Extru_200, which explains of the improvement in creep resistance. The calculated activation energy of the samples, as presented in the SI and Table 7, indicates a lower value for the pristine PBT sample (28.8 $kJ.mol^{-1}$) compared to the Extru_50 sample (58.7 $kJ.mol^{-1}$). This suggests that a greater amount of energy is required for solid vitrimerized PBT to flow. The Extru_100 and Extru_200 samples exhibited progressively lower activation energies, with the extrusion at 200 rpm approaching the PBT (33.8 $kJ.mol^{-1}$). This suggests that gelation was hindered during extrusion, and some improvement in the rheological properties was observed due to vitrimerization. The higher the crosslink density, the better the creep resistance and the lower the permanent deformation. Additionally, the instantaneous strain recovery of vitrimerized formulations has been observed to be lower than that of pristine PBT at 160°C. However, at 180°C or 200°C, the instantaneous strain recovery became equivalent to that of pristine PBT. This is probably due to the activation of bond exchanges, which, in the case of vitrimerized networks, occurs at a rate fast enough to be detected at the measurement time scale.[3,62,63]

Table 7 Activation energies calculated from creep data

	E_a ($kJ.mol^{-1}$) - creep
PBT	28.8
50rpm	58.7
100 rpm	41.7
200 rpm	33.8

The last point to be addressed from the experimental data analysis was the effect of the screw rotation speed on the mechanical properties of the samples. As shown by the WAXS data, a crystal orientation was detected at the skin mold

predominantly in Extru_50 but also in Extru_100 prepared by injection. The injection time (1.2 s) was the same for all specimens used for the WAXS measurements (shown in Figure 6B and Figure 66C). Therefore, it can be reasonably assumed that the velocity and shear strain rate profiles ($v(x)$ and $\dot{\gamma}(x)$) are also identical. This means that the difference in shear stress causing the difference in polymer orientation observed in Figures 6B and 6C is due to the viscosity magnitude in Equation 1. As shown in the melt rheology (Figure2A), the modulus values of these materials were significantly different at both the extruder outlet (t=0 in Figure 2A) and after crosslinking in the micro-compounder before injection (t=5 mins in figure 2A). All these formulations presented higher viscosity and therefore, upon injection, the polymer chains tended to align in the injection direction. This suggests that the anisotropy identified through XRD has a significant influence on the reinforcement of the vitrimer mechanical properties, which would thus be an 'indirect' effect of vitrimerization. To confirm this, samples (from the Extru_50 formulation) were injection-molded at different speed rates (injection time = 2.6s). In this case, the material is the same in the molten state and the terms that changes in equation 1 is $\dot{\gamma}(x)$ related to the injection speed. Figure 8 shows that the injection speed has a significant influence on the mechanical properties of the specimen. The Young's modulus and the strain hardening modulus measured for an injection time of 2.6s are E=383 MPa and Gr=6.45 MPa while for an injection time of 1.2s they are 538 MPa and 13.5 MPa. This is due to the increase in shear rate $\dot{\gamma}$ that causes higher degree of polymer orientation.

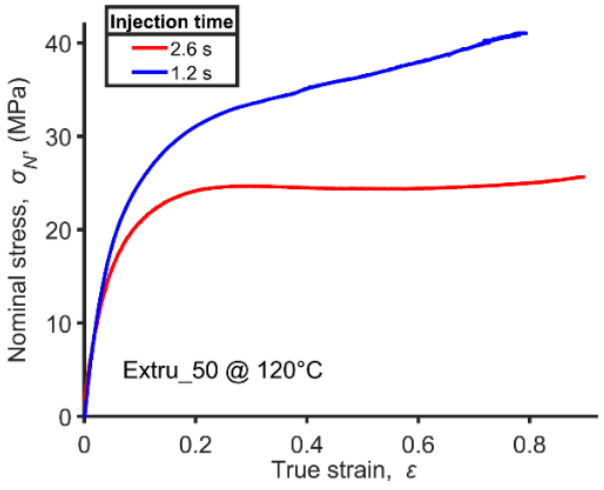

Figure 8 (Color online) $\sigma_N(\varepsilon)$ curves measured at 120°C for extru_50 at injection times of 1.2 s and 2.6 s respectively.

Hence, the degree of polymer orientation had a significant effect on the tensile properties of the vitrimerized PBT above the glass transition temperature of the network (120°C). This effect, combined with the increase of strain hardening related to the presence of dynamic crosslinks in PBT matrices,[14,20] makes the tensile properties of PBT at high temperature significantly higher after vitrimerization. However, for the data at 20°C (Figure 4A), all vitrimerized samples exhibit a higher yield stress ($\sigma_y \approx 60MPa$ vs. $\sigma_y \approx 38MPa$ for pristine PBT at equivalent strain). In terms of testing, when the amorphous phase of PBT was not mobile (below its glass transition temperature), a clear effect of the formation of a branched/crosslinked network was observed. The 3D network reduces the mobility of the polymer chains within the amorphous phase of PBT, making it more resilient to tensile deformation in its glassy state. This behavior does not seem to be significantly affected by the anisotropy of the material, as the difference between the vitrimerized samples is much less pronounced that when testing is carried out at 120°C.

In terms of vitrimers, it is relatively important to consider how the networks extruded at 100 rpm and 200 rpm can be categorized, and whether there is any interest in developing such networks. From the tensile test conducted at T = 20°C, the work of fracture (W_f) was determined by integrating the area under the nominal stress-strain curve (Figure S15);[64] the results are summarized in Table S4. For the crosslinked samples (Ref_{100} and Extru_50), the W_f was noticeably lower than that of the unaltered PBT, at 61% and 84% of the initial W_f of the unaltered PBT, respectively. This decrease in W_f suggests that the higher crosslink density in these samples contributes to increased material rigidity and brittleness, which are associated with a reduced ability to absorb energy prior to fracture. The samples where the extrusion process hampered crosslinking (Extru_100 and Extru_200) showed a significant increase in W_f, with 43% and 51% increases, respectively, compared to the pristine PBT. This increase in W_f suggests that the network formed during the extrusion process effectively enhanced the resistance of the material to deformation. This behavior is similar to the effects observed in chain-extended polymers, where increased molecular weight or alterations in the polymer architecture can lead to improved mechanical properties. In our case, the absence of gelation led to increased mobility of the extended and/or branched molecular chains, leading to an improved ability to withstand deformation rendering vitrimerized PBT interesting in term of resistance to fracture. Additionally, the minimal difference in W_f between Extru_100 and Extru_200 suggests that the degree of chain scission occurring during the extrusion process does not significantly impact W_f, provided that gelation of the network remains incomplete. This observation highlights the delicate balance between the crosslinking and chain scission

processes in determining the mechanical performance of the vitrimerized PBT materials.

It should also be noted that those specimen (Extru_100 and Extru_200) can undergo some branching through transesterification, hence, vitrimerized PBT extruded at high shear rates still retains certain properties of the vitrimerized thermoplastics. The increase in the moduli (G' and G'', Figures 2 and S3) of the molten polymer and the improved creep resistance are typical of dynamic crosslinking. Despite not being fully crosslinked, these formulations possess dynamic covalent bonds in the form of a branched micro-vitrimers, with rheological and morphological differences compared to the PBT polymer. In this sense, Extru_100 exhibits interesting properties that make it capable of holding its shape upon small deformation, while flowing like a liquid during processing at high speed or higher temperature. To demonstrate the interest of such a formulation, Extru_100 was used to produce a 3D printed complex structure by fused filament fabrication. Usually, the crosslinking of in vitrimers renders the material too viscous to be formed as a filler or 3D printed by such a technique, while the high melt flow index of PBT necessitates blending with other thermoplastics or fillers to render it printable.[36] However, the properties of Extru_100 make the material perfectly suitable for this application, allowing the printing of complex structures such as Schwarz P without the use of solvent or other complexifying procedures (Figure S16). Recent studies on processable vitrimers have focused on the use of blends with different chemistries, which can be complex to prepare.[65–67] In this study, only the mechanical parameters during the processes controlled the final flow properties of the materials.

5. Conclusion

The vitrimerization of thermoplastics is often portrayed as a straightforward process that is compatible with classical thermoplastics processing methods. However, vitrimerization fundamentally alters the rheological behavior of thermoplastic polymers, changing the manner in which the polymer network flows. Once crosslinking is achieved, the fluidity of the thermoplastic switches from viscous to a more elastic behavior, increasing the energy and time required for processing. In addition, vitrimerization at a high shear rate results in competition between the branching/crosslinking reaction and the shear-induced chain scissions. A higher shear stress increases the prevalence of shear-induced chain scissions, resulting in the inability to form a 3D network required to get a vitrimer. Instead, the network processed at a high shear stress will be formed of small micro-vitrimers that are not connected as a whole. The network can recover some of its connectivity through transesterification, leading to an increase in the viscosity and mechanical properties. This is a promising approach for recycling end-of-life thermoplastics by applying a vitrimerizing process that is suitable to high-volume processes. However, a trade-off must be considered between the extrusion rate and the crosslink density. Further studies could lead to the determination of the limiting shear stress factor for each type of polymer used relative to the entanglement level and crosslink density.

With this type of parameter, it is possible to control the decrease in the crosslink density and predict the rheological behavior of the polymer network. This mechanism of degradation (chain scission) leads to a transition from a polymer network with typical vitrimer properties to a branched non-crosslinked polymer comprising exchangeable covalent bonds with flow properties of a thermoplastics. Depending on the degree of chain scission, the structural integrity of the melted polymer can be retained at a low strain rate (viscoelastic solid) and behaves like a viscoelastic liquid at a higher strain rate. This demonstrates the potential of these materials for extending the range of processing techniques in which vitrimerized polymers can be used. A partially crosslinked network (here Extru_100) still shows interesting potential, exhibiting solid behavior above the melting of crystals when no deformation is applied and good flowability upon application of stress, making them compatible with techniques such as fused filament fabrication. However, further studies are needed to confirm that this new composition is not sensitive to long-term degradation, such as exposure to moisture, or is more prone to thermal degradation. The current study shows that properties can be tuned using only mechanical parameters, and that the improvement of mechanical properties by vitrimerization should not be considered strictly from crosslinking, but also from the possible development of anisotropy induced by viscosity evolution during processes, which offers interesting perspectives for designing material properties.

Conflict of interest

There is no conflict of interest to declare

CRediT author statement

Q.-A. Poutrel : Conceptualization, Methodology, Validation, Formal analysis, Investigation, Data curation, Writing – Original Draft/Review & Editing, Visualization; R. Kmo : Investigation, Validation, Visualization; A. Cohadon : Investigation, Validation, Formal analysis, Methodology, Writing – Review & Editing; J. Boisse : Formal analysis, Data curation, Visualization; S. Rouziere : Resources; S. Andre : Resources, Project administration, Writing – Review & Editing ; S. Hoppe : Investigation, Resources, Project administration, Writing –

Review & Editing, Funding acquisition ; L. Farge: Investigation, Validation, Formal analysis, Data curation, Visualization, Resources, Project administration, Writing – Review & Editing, Funding acquisition

Acknowledgement

The authors would like to thank the Grand Est Region and ADEME (French agency for ecological transition) for their financial support – Grant N°21GED0382. Our thanks also go to Richard Comte, engineer at Halle des Matériaux (Ecole Européenne d'Ingénieurs en Génie des Matériaux - EEIGM) for his help in preparing very thin slices of our polymer/vitrimer samples in view of WAXS experiments.

References

(1) Denissen, W.; Winne, J. M.; Du Prez, F. E. Vitrimers: Permanent Organic Networks with Glass-like Fluidity. *Chem. Sci.* **2016**, *7* (1), 30–38. https://doi.org/10.1039/C5SC02223A.

(2) Krishnakumar, B.; Sanka, R. V. S. P.; Binder, W. H.; Parthasarthy, V.; Rana, S.; Karak, N. Vitrimers: Associative Dynamic Covalent Adaptive Networks in Thermoset Polymers. *Chem. Eng. J.* **2020**, *385* (July 2019), 123820. https://doi.org/10.1016/j.cej.2019.123820.

(3) Montarnal, D.; Capelot, M.; Tournilhac, F.; Leibler, L. Silica-Like Malleable Materials from Permanent Organic Networks. *Science (80-.).* **2011**, *334* (6058), 965–968. https://doi.org/10.1126/science.1212648.

(4) Lessard, J. J.; Garcia, L. F.; Easterling, C. P.; Sims, M. B.; Bentz, K. C.; Arencibia, S.; Savin, D. A.; Sumerlin, B. S. Catalyst-Free Vitrimers from Vinyl Polymers. *Macromolecules* **2019**, *52* (5), 2105–2111. https://doi.org/10.1021/acs.macromol.8b02477.

(5) Denissen, W.; Rivero, G.; Nicolaÿ, R.; Leibler, L.; Winne, J. M.; Du Prez, F. E. Vinylogous Urethane Vitrimers. *Adv. Funct. Mater.* **2015**, *25* (16), 2451–2457. https://doi.org/10.1002/adfm.201404553.

(6) Tretbar, C. A.; Neal, J. A.; Guan, Z. Direct Silyl Ether Metathesis for Vitrimers with Exceptional Thermal Stability. *J. Am. Chem. Soc.* **2019**, *141* (42), 16595–16599. https://doi.org/10.1021/jacs.9b08876.

(7) Zhang, S.; Pan, L.; Xia, L.; Sun, Y.; Liu, X. Dynamic Polysulfide Shape Memory Networks Derived from Elemental Sulfur and Their Dual Thermo-/Photo-Induced Solid-State Plasticity. *React. Funct. Polym.* **2017**, *121*, 8–14. https://doi.org/10.1016/j.reactfunctpolym.2017.10.005.

(8) Niu, X.; Wang, F.; Kui, X.; Zhang, R.; Wang, X.; Li, X.; Chen, T.; Sun, P.; Shi, A. Dual Cross-linked Vinyl Vitrimer with Efficient Self-Catalysis Achieving Triple-Shape-Memory Properties. *Macromol. Rapid Commun.* **2019**, *40* (19). https://doi.org/10.1002/marc.201900313.

(9) Delahaye, M.; Winne, J. M.; Du Prez, F. E. Internal Catalysis in Covalent Adaptable Networks: Phthalate Monoester Transesterification As a Versatile Dynamic Cross-Linking Chemistry. *J. Am. Chem. Soc.* **2019**, *141* (38), 15277–15287. https://doi.org/10.1021/jacs.9b07269.

(10) Chen, Q.; Yu, X.; Pei, Z.; Yang, Y.; Wei, Y.; Ji, Y. Multi-Stimuli Responsive and Multi-Functional Oligoaniline-Modified Vitrimers. *Chem. Sci.* **2017**, *8* (1), 724–733. https://doi.org/10.1039/C6SC02855A.

(11) Yang, Z.; Wang, Q.; Wang, T. Dual-Triggered and Thermally Reconfigurable Shape Memory Graphene-Vitrimer Composites. *ACS Appl. Mater. Interfaces* **2016**, *8* (33), 21691–21699. https://doi.org/10.1021/acsami.6b07403.

(12) Chen, G.; Wu, K.; Zhang, Q.; Shi, Y.; Lu, M. Dual-Responsive Shape Memory and Thermally Reconfigurable Reduced Graphene Oxide-Vitrimer Composites. *Macromol. Res.* **2019**, *27* (6), 526–533. https://doi.org/10.1007/s13233-019-7080-x.

(13) Qiu, J.; Ma, S.; Wang, S.; Tang, Z.; Li, Q.; Tian, A.; Xu, X.; Wang, B.; Lu, N.; Zhu, J. Upcycling of Polyethylene Terephthalate to Continuously Reprocessable Vitrimers through Reactive Extrusion. *Macromolecules* **2021**, *54* (2), 703–712. https://doi.org/10.1021/acs.macromol.0c02359.

(14) Farge, L.; Spiegel, R.; André, S.; Noûs, C.; Lainé, R.; Hoppe, S. Development of Plasticity in Vitrimers Synthesized from a Semi-crystalline Polymer Using Injection Molding. *J. Polym. Sci.* **2022**, *60* (13), 1962–1975. https://doi.org/10.1002/pol.20220062.

(15) Demongeot, A.; Groote, R.; Goossens, H.; Hoeks, T.; Tournilhac, F.; Leibler, L. Cross-Linking of Poly(Butylene Terephthalate) by Reactive Extrusion Using Zn(II) Epoxy-Vitrimer Chemistry. *Macromolecules* **2017**, *50* (16), 6117–6127. https://doi.org/10.1021/acs.macromol.7b01141.

(16) Caffy, F.; Nicolaÿ, R. Transformation of Polyethylene into a Vitrimer by Nitroxide Radical Coupling of a Bis-Dioxaborolane. *Polym. Chem.* **2019**, *10* (23), 3107–3115. https://doi.org/10.1039/C9PY00253G.

(17) Röttger, M.; Domenech, T.; van der Weegen, R.; Breuillac, A.; Nicolaÿ, R.; Leibler, L. High-Performance Vitrimers from Commodity Thermoplastics through Dioxaborolane Metathesis. *Science (80-.).* **2017**, *356* (6333), 62–65. https://doi.org/10.1126/science.aah5281.

(18) Loyer, C.; Régnier, G.; Duval, V.; Ould, Y.; Richaud, E. PBT Plasticity Loss Induced by Oxidative and Hydrolysis Ageing. *Polym. Degrad. Stab.* **2020**, *181* (109368). https://doi.org/10.1016/j.polymdegradstab.2020.109368.

(19) Zhou, Z.; Yin, N.; Zhang, Y.; Zhang, Y. Properties of Poly(Butylene Terephthalate) Chain-Extended by Epoxycyclohexyl Polyhedral Oligomeric Silsesquioxane. *J. Appl. Polym. Sci.* **2007**, *107*, 825–830. https://doi.org/10.1002/app.

(20) Farge, L.; Hoppe, S.; Daujat, V.; Tournilhac, F.; André, S. Solid Rheological Properties of PBT-Based Vitrimers. *Macromolecules* **2021**, *54* (4), 1838–1849. https://doi.org/10.1021/acs.macromol.0c02105.

(21) Zhou, Y.; Goossens, J. G. P.; Sijbesma, R. P.; Heuts, J. P. A. Poly(Butylene Terephthalate)/Glycerol-Based Vitrimers via Solid-State Polymerization. *Macromolecules* **2017**, *50* (17), 6742–6751. https://doi.org/10.1021/acs.macromol.7b01142.

(22) Vergnes, B.; Chapet; M. Extrusion - Procedes d'extrusion Bivis. *Techniques de l'ingenieur*; 2001.

(23) Martin, P.; Devaux, J.; Legras, R.; Leemans, L.; Van Gurp, M.; Van Duin, M. Complex Processing-Morphology Interrelationships During the Reactive Compatibilization of Blends of Poly(Butylene Terephthalate) with Epoxide-Containing Rubber. *J. Appl. Polym. Sci.* **2004**, *91* (2), 703–718. https://doi.org/10.1002/app.13052.

(24) Nelson, A. Z.; Wang, Y.; Wang, Y.; Margotta, A. S.; Sammler, R. L.; Izmitli, A.; Katz, J. S.; Curtis-Fisk, J.; Li, Y.; Ewoldt, R. H. Gelation under Stress: Impact of Shear Flow on the Formation and Mechanical Properties of Methylcellulose Hydrogels. *Soft Matter* **2022**, *18* (7), 1554–1565. https://doi.org/10.1039/D1SM01711J.

(25) Izak-Nau, E.; Demco, D. E.; Braun, S.; Baumann, C.; Pich, A.; Göstl, R. Shear-Induced Structural and Functional Transformations of Poly(N -Vinylcaprolactam) Microgels. *ACS Appl. Polym. Mater.* **2020**, *2* (4), 1682–1691. https://doi.org/10.1021/acsapm.0c00111.

(26) Scaffaro, R.; La Mantia, F. P.; Botta, L.; Morreale, M.; Tz. Dintcheva, N.; Mariani, P. Competition between Chain Scission and Branching Formation in the Processing of High-density Polyethylene: Effect of Processing Parameters and of Stabilizers. *Polym. Eng. Sci.* **2009**, *49* (7), 1316–1325. https://doi.org/10.1002/pen.21317.

(27) Nasr, A.; Svoboda, P. Influence of Thermal Degradation on the Crystallization of Poly(Butylene Terephthalate). *Express Polym. Lett.* **2024**, *18* (3), 309–325. https://doi.org/10.3144/expresspolymlett.2024.22.

(28) Courtat, J. Étude De La Fonctionnalisation De Charges Minérales Pré- Formées Pour La Formation De Matériaux Polymères En Vue D'Une Tenue Au Feu Améliorée Pour Un Remplacement, À Terme, Des Charges Halogénées Actuelles, Matériaux. Université Claude Bernard - Lyon I, 2014. Français. <NNT : 2014LYO10326> <tel-01131378>. https://theses.hal.science/tel-01131378.

(29) Salavati-Niasari, M.; Gholami-Daghian, M.; Esmaeili-Zare, M.; Sangsefidi, F. S. Solid State Synthesis and Characterization of Zinc Oxide (ZnO) Microflakes by [Bis(Acetylacetonato)Zinc(II)] and Sodium Hydroxide at Room Temperature. *J. Clust. Sci.* **2013**, *24* (4), 1093–1101. https://doi.org/10.1007/s10876-013-0600-5.

(30) Wang, Z.; Cui, Y.-T.; Xu, Z.-B.; Qu, J. Hot Water-Promoted Ring-Opening of Epoxides and Aziridines by Water and Other Nucleopliles. *J. Org. Chem.* **2008**, *73* (6), 2270–2274. https://doi.org/10.1021/jo702401t.

(31) Rouzière, S.; Jourdanneau, E.; Kasmi, B.; Joly, P.; Petermann, D.; Albouy, P. A. A Laboratory X-Ray Microbeam for Combined X-Ray Diffraction and Fluorescence Measurements. *J. Appl. Crystallogr.* **2010**, *43* (5), 1131–1133. https://doi.org/10.1107/S0021889810027901.

(32) Langford, J. I.; Wilson, A. J. C. Scherrer after Sixty Years: A Survey

and Some New Results in the Determination of Crystallite Size. *J. Appl. Crystallogr.* **1978**, *11* (2), 102–113. https://doi.org/10.1107/S0021889878012844.

(33) Goderis, B.; Reynaers, H.; Scherrenberg, R.; Mathot, V. B. F.; Koch, M. H. J. Temperature Reversible Transitions in Linear Polyethylene Studied by TMDSC and Time-Resolved, Temperature-Modulated WAXD/SAXS. *Macromolecules* **2001**, *34* (6), 1779–1787. https://doi.org/10.1021/ma001759y.

(34) Strobl, G. Colloquium: Laws Controlling Crystallization and Melting in Bulk Polymers. *Rev. Mod. Phys.* **2009**, *81* (3), 1287–1300. https://doi.org/10.1103/RevModPhys.81.1287.

(35) Vidil, T.; Tournilhac, F.; Musso, S.; Robisson, A.; Leibler, L. Control of Reactions and Network Structures of Epoxy Thermosets. *Prog. Polym. Sci.* **2016**, *62*, 126–179. https://doi.org/10.1016/j.progpolymsci.2016.06.003.

(36) Borman, W. F. H. Molecular Weight–Viscosity Relationships for Poly(1,4-butylene Terephthalate). *J. Appl. Polym. Sci.* **1978**, *22* (8), 2119–2126. https://doi.org/10.1002/app.1978.070220804.

(37) Konishi, T.; Sakatsuji, W.; Fukao, K.; Miyamoto, Y. Temperature Dependence of Lamellar Thickness in Isothermally Crystallized Poly(Butylene Terephthalate). *Macromolecules* **2016**, *49* (6), 2272–2280. https://doi.org/10.1021/acs.macromol.6b00126.

(38) Xanthos, M. Reactive Modification/Compatibilization of Polyesters. In *Handbook of Thermoplastic Polyesters*; Wiley, 2002; Vol. 19, pp 815–833.

(39) Lomellini, P. Effect of Chain Length on the Network Modulus and Entanglement. *Polymer (Guildf).* **1992**, *33* (6), 1255–1260. https://doi.org/10.1016/0032-3861(92)90771-N.

(40) Yarusso, D. J. Effect of Rheology on PSA Performance. In *Adhesion Science and Engineering*; Elsevier, 2002; pp 499–533. https://doi.org/10.1016/B978-0-444-51140-9.50040-8.

(41) Rudin, A.; Choi, P. Mechanical Properties of Polymer Solids and Liquids. In *The Elements of Polymer Science & Engineering*; Elsevier, 2013; pp 149–229. https://doi.org/10.1016/B978-0-12-382178-2.00004-3.

(42) Haward, R. N. Strain Hardening of Thermoplastics. *Macromolecules* **1993**, *26* (22), 5860–5869. https://doi.org/10.1021/ma00074a006.

(43) Farge, L.; Tournilhac, F.; Hoppe, S.; Perez, J.; Bihannic, I.; Bianchin, J.; Poutrel, Q.-A.; Boisse, J.; André, S. Deformation Mechanisms in PBT at Elevated Temperatures. *Mater. Today Commun.* **2023**, *36* (July), 106774. https://doi.org/10.1016/j.mtcomm.2023.106774.

(44) Strobl, G. *The Physics of Polymers*; Springer Berlin Heidelberg: Berlin, Heidelberg, 2007. https://doi.org/10.1007/978-3-540-68411-4.

(45) Cao, W.; Wang, K.; Zhang, Q.; Du, R.; Fu, Q. The Hierarchy Structure and Orientation of High Density Polyethylene Obtained via Dynamic Packing Injection Molding. *Polymer (Guildf).* **2006**, *47* (19), 6857–6867. https://doi.org/10.1016/j.polymer.2006.07.037.

(46) Yokouchi, M.; Sakakibara, Y.; Chatani, Y.; Tadokoro, H.; Tanaka, T.; Yoda, K. Structures of Two Crystalline Forms of Poly(Butylene Terephthalate) and Reversible Transition between Them by Mechanical Deformation. *Macromolecules* **1976**, *9* (2), 266–273. https://doi.org/10.1021/ma60050a018.

(47) Schrauwen, B. A. G.; Breemen, L. C. A. V.; Spoelstra, A. B.; Govaert, L. E.; Peters, G. W. M.; Meijer, H. E. H. Structure, Deformation, and Failure of Flow-Oriented Semicrystalline Polymers. *Macromolecules* **2004**, *37* (23), 8618–8633. https://doi.org/10.1021/ma048884k.

(48) Pritchard, R. H.; Redmann, A.-L.; Pei, Z.; Ji, Y.; Terentjev, E. M. Vitrification and Plastic Flow in Transient Elastomer Networks. *Polymer (Guildf).* **2016**, *95*, 45–51. https://doi.org/10.1016/j.polymer.2016.04.060.

(49) Poutrel, Q.-A.; Blaker, J. J.; Soutis, C.; Tournilhac, F.; Gresil, M. Dicarboxylic Acid-Epoxy Vitrimers: Influence of the off-Stoichiometric Acid Content on Cure Reactions and Thermo-Mechanical Properties. *Polym. Chem.* **2020**, *11* (33), 5327–5338. https://doi.org/10.1039/D0PY00342E.

(50) Vidil, T.; Cloître, M.; Tournilhac, F. Control of Gelation and Network Properties of Cationically Copolymerized Mono- and Diglycidyl Ethers. *Macromolecules* **2018**, *51* (14), 5121–5137. https://doi.org/10.1021/acs.macromol.8b00406.

(51) Huang, J.; Fu, P.; Li, W.; Xiao, L.; Chen, J.; Nie, X. Influence of Crosslinking Density on the Mechanical and Thermal Properties of Plant Oil-Based Epoxy Resin. *RSC Adv.* **2022**, *12* (36), 23048–23056. https://doi.org/10.1039/D2RA04206A.

(52) Barszczewska-Rybarek, I. M.; Korytkowska-Wałach, A.; Kurcok, M.; Chladek, G.; Kasperski, J. DMA Analysis of the Structure of Crosslinked Poly(Methyl Methacrylate)S. *Acta Bioeng. Biomech.* **2017**, *19* (1), 47–53. https://doi.org/10.5277/ABB-00590-2016-01.

(53) Huang, K.; Zhang, P.; Zhang, J.; Li, S.; Li, M.; Xia, J.; Zhou, Y. Preparation of Biobased Epoxies Using Tung Oil Fatty Acid-Derived C21 Diacid and C22 Triacid and Study of Epoxy Properties. *Green Chem.* **2013**, *15* (9), 2466. https://doi.org/10.1039/c3gc40622a.

(54) Samperi, F.; Puglisi, C.; Alicata, R.; Montaudo, G. Thermal Degradation of Poly(Butylene Terephthalate) at the Processing Temperature. *Polym. Degrad. Stab.* **2004**, *83* (1), 11–17. https://doi.org/10.1016/S0141-3910(03)00167-8.

(55) Kosky, P. G.; Mcdonald, S.; Guggenheim, A. Determination of End-Group Concentrations and Molecular Weight of Poly(Buty1ene Terephthalate) by Solid-State Fourier Transform Infrared Spectroscopy. *Polym. Eng. Sci.* **1985**, *25* (7), 389–394. https://doi.org/10.1002/pen.760250703.

(56) Martinez-Garcia, J. C.; Rzoska, S. J.; Drozd-Rzoska, A.; Starzonek, S.; Mauro, J. C. Fragility and Basic Process Energies in Vitrifying Systems. *Sci. Rep.* **2015**, *5* (1), 8314. https://doi.org/10.1038/srep08314.

(57) Ricarte, R. G.; Tournilhac, F.; Cloître, M.; Leibler, L. Linear Viscoelasticity and Flow of Self-Assembled Vitrimers: The Case of a Polyethylene/Dioxaborolane System. *Macromolecules* **2020**, *53* (5), 1852–1866. https://doi.org/10.1021/acs.macromol.9b02415.

(58) Ricarte, R. G.; Tournilhac, F.; Leibler, L. Phase Separation and Self-Assembly in Vitrimers: Hierarchical Morphology of Molten and Semicrystalline Polyethylene/Dioxaborolane Maleimide Systems. *Macromolecules* **2019**, *52* (2), 432–443. https://doi.org/10.1021/acs.macromol.8b02144.

(59) Tangthana-umrung, K.; Poutrel, Q. A.; Gresil, M. Epoxy Homopolymerization as a Tool to Tune the Thermo-Mechanical Properties and Fracture Toughness of Vitrimers. *Macromolecules* **2021**, *54* (18), 8393–8406. https://doi.org/10.1021/acs.macromol.1c00861.

(60) Tangthana-umrung, K.; Gresil, M. Interlaminar Fracture Toughness Behaviour of Carbon Fibre Reinforced Polymer with Epoxy-Dicarboxylic Acid Vitrimer Matrix. **2022**, *32* (November 2021).

(61) Pillin, I.; Pimbert, S.; Feller, J.; Levesque, G. Crystallization Kinetics of Poly(Butylene Terephthalate) (PBT): Influence of Additives and Free Carboxylic Acid Chain Ends. *Polym. Eng. Sci.* **2001**, *41* (2), 178–191. https://doi.org/10.1002/pen.10720.

(62) Liu, W.; Schmidt, D. F.; Reynaud, E. Catalyst Selection, Creep, and Stress Relaxation in High-Performance Epoxy Vitrimers. *Ind. Eng. Chem. Res.* **2017**, *56* (10), 2667–2672. https://doi.org/10.1021/acs.iecr.6b03829.

(63) Demongeot, A.; Mougnier, S.-J. J.; Okada, S.; Soulié-Ziakovic, C.; Tournilhac, F. Coordination and Catalysis of Zn 2+ in Epoxy-Based Vitrimers. *Polym. Chem.* **2016**, *7* (27), 4486–4493. https://doi.org/10.1039/C6PY00752J.

(64) Oh, G. A Simplified Toughness Estimation Method Based on Standard Tensile Data. *Int. J. Press. Vessel. Pip.* **2022**, *199* (June 2021), 104733. https://doi.org/10.1016/j.ijpvp.2022.104733.

(65) Joosten, L. M. A.; Cassagnau, P.; Drockenmuller, E.; Montarnal, D. Synthesis, Recycling and High-Throughput Reprocessing of Phase-Separated Vitrimer-Thermoplastic Blends. *Adv. Funct. Mater.* **2024**, *34* (1), 1–12. https://doi.org/10.1002/adfm.202306882.

(66) Kar, G. P.; Saed, M. O.; Terentjev, E. M. Scalable Upcycling of Thermoplastic Polyolefins into Vitrimers through Transesterification. *J. Mater. Chem. A* **2020**, *8* (45), 24137–24147. https://doi.org/10.1039/D0TA07339C.

(67) Ricarte, R. G.; Shanbhag, S. Unentangled Vitrimer Melts: Interplay between Chain Relaxation and Cross-Link Exchange Controls Linear Rheology. *Macromolecules* **2021**, *54* (7), 3304–3320. https://doi.org/10.1021/acs.macromol.0c02530.